Chemical Engineering Journal 472 (2023) 144980

Contents lists available at ScienceDirect

Chemical Engineering Journal

journal homepage: www.elsevier.com/locate/cej

Decellularized extracellular matrix-based 3D nanofibrous scaffolds functionalized with polydopamine-reduced graphene oxide for neural tissue engineering

Daniela M. da Silva [a,b,1], Nathalie Barroca [a,b,1,*], Susana C. Pinto [a,b], Ângela Semitela [a,b], Bárbara M. de Sousa [c], Patrícia A.D. Martins [a,d,e], Luís Nero [d,e], Iratxe Madarieta [f], Nerea García-Urkia [f], Francisco-Javier Fernández-San-Argimiro [f], Andrea Garcia-Lizarribar [f], Olatz Murua [f], Beatriz Olalde [f], Igor Bdikin [a,b], Sandra I. Vieira [c], Paula A.A.P. Marques [a,b,*]

[a] Centre for Mechanical Technology and Automation, Department of Mechanical Engineering, University of Aveiro, 3810-193, Aveiro, Portugal
[b] LASI - Intelligent Systems Associate Laboratory, 4800-058 Guimarães, Portugal
[c] iBiMED, Department of Medical Sciences, University of Aveiro, Aveiro, Portugal
[d] Department of Electronics, Telecommunications and Informatics, University of Aveiro, Aveiro, Portugal
[e] Instituto de Telecomunicações, 3810-193 Aveiro, Portugal
[f] TECNALIA, Basque Research and Technology Alliance (BRTA), E20009 Donostia-San Sebastian, Spain

ARTICLE INFO

Keywords:
Adipose-derived decellularized extracellular matrix
Graphene oxide
Neural stem cells
Gas foaming
3D nanofibrous scaffold
Neuronal regeneration

ABSTRACT

One of the exciting prospects of using decellularized extracellular matrices (ECM) lies in their biochemical profile of preserved components, many of which are regeneration-permissive. Herein, a decellularized ECM from adipose tissue (adECM) was explored to design a scaffolding strategy for the challenging repair of the neural tissue. Targeting the recreation of the nano-scaled architecture of native ECM, adECM was first processed into nanofibers by electrospinning to produce bidimensional platforms. These were further shaped into three-dimensional (3D) nanofibrous constructs by gas foaming. The conversion into a 3D microenvironment of nanofibrous walls was assisted by blending the adECM with lactide-caprolactone copolymers, wherein tuning the adECM/copolymer ratio along with the amount of caprolactone in the copolymer led to modulating the mechanical properties towards soft, yet structurally stable, 3D constructs. In view of boosting their performance to guide neural stem cell fate, adECM-based platforms were doped with a bioinspired surface modification relying on polydopamine-functionalized reduced graphene oxide (PDA-rGO). These adECM-based 3D constructs revealed a permissive microenvironment for neural stem cells (NSCs) to adhere, grow, and migrate throughout the microporosity, owing to the synergy between the unique biochemical features of the adECM and the nanofibrous architecture. NSC responded differently depending on the adECM-based architecture–nanofibrous bidimensional, or 3D design. The 3D spatial arrangement of the nanofibers – induced by the gas foaming – exhibited a remarkable effect on NSCs' phenotype determination and neurite formation, thereby reinforcing the critical importance of engineering scaffolds with multiple length-scale architecture. Furthermore, PDA-rGO promoted the differentiation of NSC towards the neuronal lineage. Specifically in 3D, it significantly increases the levels of Tuj1 and MAP2 a/b isoforms, confirming its effectiveness in boosting neuronal differentiation and neuritogenesis.

1. Introduction

Recreating the native extracellular matrix (ECM) of tissues translates into engineering platforms with biomimetic physical and chemical organizations. The native ECM of the nervous system is mainly composed by collagen, glycoproteins such as fibronectin, laminins and dystroglycan and proteoglycans like perlecan or tenascin [1]. Thus, the use of single components or combination of these ECM components have been intuitively the basis for regenerative strategies [2]. Sensibly, decellularizing extracellular matrices from different tissues to explore as building

* Corresponding authors.
E-mail addresses: nbarroca@ua.pt (N. Barroca), paulam@ua.pt (P.A.A.P. Marques).
[1] These authors contributed equally to this work.

https://doi.org/10.1016/j.cej.2023.144980
Received 13 April 2023; Received in revised form 18 July 2023; Accepted 21 July 2023
Available online 22 July 2023

blocks for tissue engineering platforms also emerged as a robust manner to yield complex site-specific combinations of biochemical and mechanical cues [3]. Distinct ECM have shown encouraging outcomes for some regenerative challenges of the neural tissue such as spinal cord injuries (SCI). Namely, ECM from human umbilical cord, porcine bladder [4], and brain [5] were exploited as injectable hydrogels which supported the migration of human mesenchymal stem cells (MSC) and the differentiation of neural stem cells (NSCs) *in vitro*, specifically promoting axonal outgrowth [4]. In rat SCI models, porcine brain decellularized matrix fostered a pro-reparative macrophages' phenotype and promoted locomotor function until 2 months after the injury [5]. Interestingly, decellularization of the optic nerve, selectively removed some axonal regrowth-inhibitory molecules while preserving some regrowth-promoting ones, leading to an optimized function of the adult optic nerve in supporting the oriented outgrowth of dorsal root ganglion (DRG) neurites [6]. A decellularized matrix from a rodent spinal cord was transformed into a porous freeze-dried sponge that acted as a neurogenic niche favorable for the targeted migration, residence and neuronal differentiation of endogenous NSCs after SCI [7].

In this work, we describe a porcine adipose-derived extracellular matrix (adECM), which is abundant, easily obtainable, and rich in basement membrane proteins. Previous proteomic analysis has demonstrated the biochemical profile of several preserved ECM components, namely laminin, fibronectin, and collagen IV, among others [8]. These proteins have been characterized as permissive components of neural regeneration, specifically critical to facilitate axon growth [6]. Particularly, laminin is a major glycoprotein of the basement membrane of neural tissues, and laminin-associated integrins seems to correlate with the regenerative state of neurons associated with axonal guidance [9]. As coating in silk nanofibrous scaffolds, laminin acted as an effective biological signal for promoting nerve cell proliferation and guide axonal growth [10]. Although individual proteins such as collagen, laminin and fibronectin have shown to be suitable as substrates for NSCs adhesion, migration, and axonal growth, blending them did not always result in upgraded strategies with better biological performances [2]. Thus, the biochemical resemblance between the adECM and the molecules known to form a permissive microenvironment for neural tissue repair does not ensure, per se, that this particular adipose-derived ECM composition will translate into such a microenvironment. Therefore, any strategies based on adECM targeting the nervous system always require appropriate cytocompatibility analysis.

Regarding the recreation of the physical architecture of the native ECM, manufacturing techniques such as electrospinning [11], electrohydrodynamic jet printing [12] and lithography [13] allow the precise engineering of two-dimensional (2D) and three-dimensional (3D) platforms across a length scale from a few micrometers down to a dozen of nanometers. Early work on micropatterned polydimethylsiloxane (PDMS) surfaces demonstrated the conciliation of neuronal cell development and differentiation of primary human stem cells by carefully engineering microgrooves in PDMS surfaces, with neurite outgrowth and efficient alignment of neurites in a pre-defined direction imposed by engineering the size in micropatterning [14]. Owing to its easiness of operation, electrospinning has been massively disseminated and used to produce scaffolds with nanosized elements. Electrospinning hybrids using decellularized extracellular matrices supported by synthetic polymers are gaining interest for diverse tissues [15], including neural tissue, peripheral [16,17] and central [18], to shape ECM-based high-volume-to-surface ratio nanoscale fibrous structure, yet with structural and mechanical integrity. ECM derived from cauda equina blended with poly(l-lactide-co-glycolide) (PLGA) and electrospun into nanostructured scaffolds, allow the survival of Schwann cells and induce longer extension of axon in the dorsal root ganglia explants than PLGA alone [18]. However, electrospun membranes are not true three-dimensional environments and can be seen as bidimensional platforms with a texturization of hundreds of nanometers in scale. Also, as they have a rather limited porosity, cell migration as well as diffusion of biomolecules can be hindered. Thus, ideally, cells within a scaffold should be surrounded by nanosized fibers while still allowing for initial migration and constant exchange of biomolecules such as nutrients and waste [19]. Furthermore, NSC cultured in 2D systems may gradually lose their capacity to differentiate into neuronal cell types, so-that alternative culture systems should be considered [20]. While the cells engage with scaffolds at the nanoscale level within the early interaction stages, a multiscale architecture design is critically relevant for orchestrating the complex regenerative mechanisms. In a lateral hemisection of a SCI, increased axon regrowth through the lesion was correlated with the cell infiltration achieved by increasing the porosity and channel number within a multichannel-like bridge [21]. Besides the self-assembling peptides which are compatible with bioactive moieties and controllable in structure formation for building multi-faceted nanoscaffolds [22], there are not many studies on three-dimensional constructs using electrospun fibers as building blocks. To cite a few, electrospun nanofibrous collagen mats were organized in a rolled-up 3D configuration that suppressed astrocyte proliferation and supported DRG neurite outgrowth *in vitro,* as well as cellular infiltration and neural fiber sprouting *in vivo* [23]. Exploiting a similar approach of rolling up electrospun mats, aligned silk fibroin nanofibers were rolled longitudinally into circular channels to test the macroscale architecture effect in an injured spinal cord. Multichannel conduits with individual channels of 570 μm diameter demonstrated permeation by newborn tissue and almost a 6-fold increase in axon length compared to single-channel conduits with a diameter of 1 mm [10]. Electrospinning was also applied to an hydrogel-like photocrosslinked gelatin methacryloyl (GelMA) to produce microfibers, subsequently organized into fiber bundles that shows superior high water content and elasticity [24]. Specific 3D geometries were self-assembled based on polycaprolactone (PCL) and gelatin electrospun nanofibers acting as physical cross-linkers of reduced graphene oxide (rGO) sheets, whereby varying the chemical composition of the nanofibers, the pore size and structural integrity of the 3D constructs could be modulated [25]. Exploiting a magnetically-assisted approach, PCL-gelatin mixed with super paramagnetic iron oxide nanoparticles were wet-electrospun to form 3D scaffolds, wherein the magnetic field controlled the microarchitectural features of the resulting porous scaffolds [26]. Another avenue for shaping electrospun nanofibers into 3D constructs involves the application of gas within the electrospun membranes to induce their expansion using either physical agents such as inert gases, CO_2 or H_2, or by chemical ones (sodium or ammonium borohydride) [27,28]. These studies focus primarily on testing the gas-induced expansion on novel materials or improving the resulting micro- and nanofeatures of the resulting 3D scaffolds [29]. Gas foaming was exploited so far for peripheral nerve repair only, where electrospun membranes of polylactic acid and silk were shaped into 3D nanofibers foams to fill nerve conduit grafts showing superior performance comparing to hollow grafts [30]. Applications targeting the soft central nervous tissue are yet to be developed.

Here, the adECM of porcine origin is shaped into bidimensional electrospun platforms via electrospinning, as well as into 3D nanofibrous constructs by gas foaming. Copolymers based on the biocompatible and biodegradable polylactic acid and polycaprolactone are exploited to support the design integrity of the adECM-based 3D scaffolds.

Additionally, graphene-based materials have proven to be versatile and multifunctional platforms for the challenging pathologies of the nervous system, from biomolecules carriers to treat neurological disorders, to neuromodulation therapeutics, down to scaffolding building blocks to bridge lesions of the spinal cord. One of their effective ability is to favor neuronal differentiation [31]. Thus, we further propose a bioinspired and simple surface modification of the adECM-based platforms, via doping the adECM with a polydopamine-functionalized reduced graphene oxide (PDA-rGO), intended to further boost their performance. Among the reductant agents used to reduce graphene oxide (GO), dopamine is a promising and green alternative to the commonly toxic

and hazardous chemicals, such as hydrazine [32-34]. In mild alkaline environment, dopamine can self-polymerize into polydopamine (PDA) with catechol groups converting in quinone groups by oxidation [35,36]. Simultaneously, the electrons release in the polymerization can participate in the reduction, with PDA molecules decorating the GO surface, yet exhibiting functional groups that will allow further interaction with other molecules [37,38].

For the repair of the central nervous system, NSCs have revealed therapeutic potential in both pre-clinical and clinical settings [39], owing to their innate ability to differentiate into mature cells, specifically functional neurons and glial cells [40]. Here, a murine immortalized NSC line is employed to test the ability of the 2D and 3D nanofibrous adECM-based platforms to support neuronal migration, growth and differentiation. Furthermore, the effect of doping the platforms with functionalized rGO is investigated under distinct cell differentiation conditions.

2. Materials and methods

2.1. Materials

The polymer PURASORB® PL18, and two copolymers PURASORB® PLC8516 and PURASORB® PLC7015, were obtained from Corbion, with a lactide/caprolactone ratio of 100/0, 85/15 and 70/30 and inherent viscosities of 1.8, 1.6 and 1.5 g/mL, respectively. They are here referred as PLA100, PLA85 and PLA70, with relation to PLA content. adECM was obtained from the decellularization of the porcine adipose tissue as described previously [8]. Briefly, porcine adipose tissue was harvested from a local food company (JAUCHA S.L., Navarra, Spain), cleaned, creamed using a beater and stored at − 20 °C. Afterwards, protein pellet was obtained by tissue homogenization (Polytron PT3100) at 12,000 rpm for 5 min, centrifugation (5000 rpm for 5 min) with ultrapure water and manual discarding of lipids. Then, the protein pellet was treated with isopropanol (Merck Life Science SL, Madrid, Spain) and 1 % (v/v) triton x-100 and 0.1 % (v/v) ammonium hydroxide (Merck Life Science SL). Each step was followed by cleaning with Phosphate Buffer Saline (PBS) (Merck Life Science SL) supplemented with 1 % (v/v) antibiotic antimycotic solution (Gibco-BRL, Paisley, UK) and a last wash with Ultrapure milli Q water. Finally, adECM was milled using a mixer mill (Retsch MM400, Haan, Germany) and conserved at 4 °C in a vacuum desiccator. Powdered adECM was enzymatically digested with pepsin in 0.1 N HCl by magnetic stirring for 48 h at room temperature (RT), followed by freeze-drying. 1,1,1,3,3,3-Hexafluoro-2-propanol (HFIP; purity 99.5%), sodium borohydride ($NaBH_4$) and dopamine hydrochloride were purchased from Sigma-Aldrich (Germany) and used as received. GO (4 mg/mL aqueous dispersion) was purchased from Graphenea® (Spain).

2.2. Graphene oxide functionalization with dopamine and characterization

The modification of GO with dopamine was carried out according to Xu *et al.* [36] with minor modifications. GO aqueous dispersion (4 mg/mL) was centrifuged 3 times at 12,000 rpm for 40 min, and after each cycle the supernatant was removed and replaced by Tris-HCl 0.1 M (pH 8.5). The final concentration of GO in Tris-HCl (0.1 M, pH 8.5) was adjusted to 0.5 mg/mL. Afterwards, 25 mg of dopamine hydrochloride was added to 100 mL of the GO suspension and stirred at 60 °C. After 15 min, the resulting product was collected after centrifugation and thoroughly washed with distilled water.

Fourier-transformed infrared (FTIR) on a Perkin Elmer Spectrometer in the range 500 to 4000 cm^{-1}, with 64 scans and a resolution of 4 cm^{-1}, X-ray diffraction (XRD) on a Rigaku Smartlab SE system, and Raman-FT Bruker RFS/100S were used to characterise the final sample.

2.3. Preparation of adipose-derived extracellular matrix-based bidimensional platforms by electrospinning

Three different copolymers (PLA100, PLA85 and PLA70) were used to prepare polymer-adECM blend solutions for electrospinning. The final concentration of the blends was fixed at 14 % (w/v) and the weight ratio of adECM/copolymer was first set at 60/40. The proper amount of copolymer was dissolved in 8 mL of HFIP and adECM was added thereafter. The solution was transferred to a syringe equipped with a stainless needle (22G) and fed at a constant rate of 1.0 mL/h. NANON-01A electrospinning setup was used applying voltages at 18 to 20 kV, according to the temperature and humidity variations inside the electrospinning chamber (21 ± 2 °C and 35 ± 5% RH). The nanofibrous platforms were collected on a rotative drum (2500 rpm) covered with aluminium foil and placed at 15 cm from the needle tip. On the second approach, only the PLA70 copolymer was used in formulations of varying adECM/PLA70 ratio between 60:40 to 80:20. The resulting platforms were labelled as "2D adECM/PLA(PLA content) ratio", for example, 2D adECM/PLA70 (60/40).

To prepare the 2D platforms doped with PDA-functionalized rGO, 1.5 wt% of PDA-rGO was added to the adECM-based formulations prior electrospinning. This amount was selected based on the visual observation of the appropriate dispersion within the solution. Also, higher amounts were avoided since they favored the formation of agglomerates at the tip of the needle and disturbed the stability of the jet.

2.4. Preparation of adipose-derived extracellular matrix-based three-dimensional platforms by gas foaming

The first stage regarding the gas foaming process focused on the selection of the $NaHB_4$ concentration and time of reaction. The preselection of these parameters was addressed for the electrospun adECM/PLA70 60/40 membrane. Three different concentrations 0.1, 0.25, 0.5 M were assayed. The criterion used to select these two parameters was the obtention of reproducible, highly porous yet robust constructs. Bidimensional electrospun nanofibrous platforms were cut into 10 × 10 mm^2 pieces and immersed in freshly prepared 0.25 M $NaHB_4$ solutions for 60 s at RT. Immediately after, the 3D structures were thoroughly washed 3 times with distilled water and freeze-dried. The resulting 3D nanofibrous scaffolds were labelled similarly to their 2D counterparts.

2.5. Characterization of adipose-derived extracellular matrix based bidimensional and three-dimensional platforms

The morphology of 2D and 3D platforms was evaluated by scanning electron microscopy (SEM, Hitachi TM 4000, Japan). The average fibre diameter of the 2D nanofibrous membranes was determined from 100 measurements on each sample using SEM micrographs at a 1,000 × magnification, while the interlayer spacing (side length and width) was determined from 120 measurements using a 50 × magnification. All these measurements were carried out using Image J software (National Institutes of Health by Wayne Rasband USA).

Structural analyses included FTIR analysis, differential scanning calorimetry (DSC) and mechanical tests. FTIR spectra of the samples were recorded using a Perkin Elmer Spectrometer from 4000 to 500 cm^{-1} at a resolution of 4 cm^{-1} and 64 scans. Thermal analysis was carried out in a differential scanning calorimeter (Perkin Elmer 4000) by heating the samples from 25 °C to 220 °C with a rate of 10°/min in a N_2 atmosphere. Mechanical tests were conducted in a Instron 101 N machine (Shimadzu MMT-101 N, Japan). The mechanical strength of the 2D platforms (rectangles of 25 × 5 mm × thickness - approximately 120–200 μm) was determined in tensile mode, at a crosshead speed of 1 mm/min. The compressive behaviour of the 3D structures was carried out at 1 mm/min for full compression. Prior to the compression test, a preload of 0.01 N was applied to confirm the contact and avoid slipping.

The wettability of 2D and 3D structures was measured by assessing the angle formed between a 2 μL water drop and the material surface (sessile drop) using OCA Dataphysics (Data Physics Corp., San Jose, CA). The contact angle was measured right after the contact and monitored for more 30 s (the time that the water drop takes to be fully absorbed).

The water uptake (*WU*) was determined for 3D scaffolds by gravimetric route. The dry 3D scaffolds were weighted (W_0), immersed in PBS and kept at 37 °C. The swollen samples were removed from PBS and weighed after removing the excess surface liquid (W_t) at different time points. The samples were placed in solution again and the procedure was repeated until the swelling equilibrium was reached.

$$WU = \frac{W_t - W_0}{W_0}$$

Two selected 3D platforms were also analysed by electrochemical impedance spectroscopy to measure the effect of the PDA-functionalized rGO on the platform electrical conductivity. Briefly, the platforms were hydrated in deionized water, 3 μS/cm, and were electrically stimulated with 50 mV sinusoidal voltage signal from 1 to 1 MHz, using PalmSens4 interface (PalmSens Compact Electrochemical Interfaces, The Netherlands) to acquire the electrochemical impedance spectroscopy results. The signal was injected through platinum wires connected to silver electrodes on the top and the bottom parts of the platforms.

2.6. Neural stem cells morphology, proliferation and differentiation on the bidimensional and three-dimensional ECM based platforms

2.6.1. Cell culture and seeding

The NE-4C neuronal cell line obtained from ATCC (#CRL-2925) was used. These NSCs were maintained on poly-L-lysine (PLL, 15 μg per mL; Sigma-Aldrich)-coated culture flasks with complete culture medium: Eagle's Minimum Essential Medium (EMEM, Sigma-Aldrich) with 10% (v/v) fetal bovine serum (FBS, Sigma-Aldrich) and 1% (v/v) penicillin/streptomycin (P/S, Sigma Aldrich), at 37 °C in humidified atmosphere of 5% CO_2. Medium was replaced every second day. Prior to cell culture, the bidimensional and three-dimensional platforms were disinfected with 70% (v/v) ethanol aqueous solution, further sterilized under UV radiation for 30 min and then thoroughly washed with PBS (Panreac AppliChem). The platforms were then immersed into a PLL aqueous solution for 2 h at RT, washed twice with PBS and finally conditioned for 2 h in complete culture medium.

NSCs were seeded on the platforms at a density of 5×10^4 and 15×10^4 cells per bidimensional and three-dimensional platforms, respectively, and incubated at 37 °C for 30 min to allow cellular attachment. Of note, NSCs seeding on the three-dimensional platforms were performed on their porous surface. Afterwards, complete medium was added, and the NSCs-seeded platforms were cultured for 14 days, with medium refreshment every second day.

2.6.2. Cell metabolic activity

Cell metabolic activity was assessed using the resazurin reduction assay. Briefly, at determined time points (at day 1, 7 and 14 of culture) the cell-seeded platforms were incubated for 4 h with fresh complete medium containing 10% (v/v) of a resazurin solution (0.1 mg per mL in PBS; ACROS Organics), at 37 °C. Later, triplicates of 100 μL per well were transferred to a 96-well plate and the resazurin to resorufin conversion was measured by spectrophotometry (Infinite 200 Pro, Tecan) at 570 nm and 600 nm. For each day, final absorbance for each sample was calculated as the ratio Abs570/Abs600nm minus the Abs570/Abs600 nm ratio of a negative control (platform without cells). The absorbance values of each cell-seeded platform after 1 day of culture was considered as 100 %, and the cellular metabolic activity on day 7 and 14 was calculated as percentages of these control values.

2.6.3. Cell morphology studies

SEM was used to visualize NSCs morphology. Briefly, after 7 days of culture, the NSCs-seeded platforms were rinsed with 0.1 M sodium cacodylate buffer (SCB, Sigma-Aldrich), then fixed with paraformaldehyde (PFA, 2.5% w/v in 0.1 M SCB; Sigma-Aldrich) and glutaraldehyde (2.5% v/v in 0.1 M SCB; TCI) for 20 min at RT, dehydrated with graded concentrations of ethanol aqueous solutions (30, 50, 70, 90 and 100% v/v), dried with hexamethyldisilazane (TCI), mounted in an aluminum stub and visualized via SEM at an accelerating voltage of 10 kV. NSCs morphology was also assessed by a phalloidin/DAPI immunocytochemical staining, where NSCs-seeded platforms were first fixed in 4 % (w/v) PFA and permeabilized with 0.5 % (v/v) Triton X-100. The 3D platforms were embedded in cryomatrix (Thermo Fisher Scientific) and sectioned transversally to the z axis in 16 μm slides in a cryostat (Leica CM 3050 S). The NSCs-seeded bidimensional and the cross-sectioned three-dimensional platforms were subsequently blocked with 5% (v/v) FBS, stained with Flash Phalloidin™ Red 594 (Biolegend) and 4′,6-diamidino-2-phenylindole (DAPI) and visualized using a fluorescence microscope (Axioimager M2, Zeiss) with magnifications of 20×/0.50 and 5×/0.125.

2.6.4. NSC differentiation

On the fourth day of culture, NSCs-seeded platforms were primed with 10^{-6} M all-trans retinoic acid (RA; Sigma-Aldrich) in a low-serum medium: EMEM with 1% (v/v) FBS and 1% (v/v) P/S. 48 h later, the medium was replaced by a serum-free differentiation medium consisting of Dulbecco's Modified Eagle Medium/Nutrient Mixture F-12 Ham (Sigma-Aldrich) supplemented with 1% (v/v) B27 (Thermo Fisher Scientific), 1% (v/v) insulin-transferrin-selenium (ITS, Sigma-Aldrich) and 1% (v/v) P/S. 6 days after RA-induced differentiation, brain-derived neurotrophic factor (BDNF, 30 ng per mL; Sigma-Aldrich) was added to the serum-free differentiation medium until the end of the culture. However, to test if our platforms have the potential to guide a spontaneous neuronal differentiation, a set of samples were cultured in non-differentiating conditions, i.e. without RA, BDNF and in medium containing 10 % (v/v) of FBS.

2.6.5. Immunocytochemical staining

Differentiated NSCs-seeded platforms were fixed (1X fixation buffer diluted from a 10X stock solution consisting of 20% (w/v) formaldehyde, 2% (v/v) glutaraldehyde, 70.4 mM Na_2HPO_4,14.7 mM KH_2PO_4, 1.37 M NaCl, and 26.8 mM KCl), permeabilized with 0.1% Triton X-100 (Fisher Scientific) in PBS for 5 min, blocked with 2% (wt/v) bovine serum albumin (BSA, Sigma-Aldrich) in PBS for 30 min, and incubated for more than 1 h at RT with primary antibodies specific against β-tubulin III (Tuj1, Biolegend) and Glial Fibrillary Acidic Protein (GFAP, Sigma-Aldrich) at 1:1000 and 1:250 dilutions, respectively. After washing with PBS, the NSCs-seeded platforms were incubated for 45 min with DyLight™488-conjugated anti-mouse (Invitrogen) and Alexa Fluor 594®-conjugated anti-chicken (Invitrogen) at 1:500 and 1:1000 dilutions, respectively, and counterstained with 3 μM DAPI (Sigma-Aldrich) for 15 min. Afterwards, NSCs-seeded platforms were mounted on glass microscope slides and observed in a LSM 810 confocal microscope (Carl Zeiss Microimaging GmbH, Jena, Germany). Differentiation was analysed using the Image J software on the confocal images ($n \geq 4$ per platform) to quantify the Tuj1 and GFAP positively stained areas with respect to the DAPI area.

2.6.6. SDS-PAGE and immunoblotting

Lysates from 15×10^4 NE-4C neural stem cells grown for 14 days on the three-dimensional platforms, under differentiation medium, were prepared by collecting and mincing the 3D structures in 1% Sodium Dodecyl Sulfate (SDS), followed by sonication and boiling for 10 min. Upon protein quantification (Pierce™ BCA Protein Assay Kit, Pierce Biotechnology), mass-normalized lysates were resolved by 5–20% gradient SDS-PAGE in Tris-Glycine buffer and electrotransferred onto nitrocellulose membranes.

After reversible incubation with Ponceau S (Sigma-Aldrich), and

blocking with 5% non-fat dry milk/TBS-T for 2 h at RT, membranes were further incubated with the primary antibodies in 3% BSA/TBS-T: mouse anti-MAP2 (Novus Biologicals NBP2-25156; 1:5000; 2 h at RT and ON at 4 °C), mouse anti-βIII-Tubulin (Sigma-Aldrich T8578; 1:4000; 2 h at RT) and mouse anti-GAPDH (Santa Cruz Biotechnology, sc-47724; 1:2000; 2 h at RT). The anti-mouse IgG secondary antibody (horseradish peroxidase-linked, Cell Signaling 7076S; 1:3000–1:5000) was then incubated (1 h at RT). The protein signal was detected by enhanced chemiluminescence (Amersham ECL Prime or ECL Select, Cytiva RPN2236 and RPN2235) using a ChemiDoc Imaging System (Bio-Rad), and results were analyzed using the ImageLab Software (Bio-Rad). The proteins' quantifications were normalized to the average of two loading controls: 1) the Ponceau S staining that assesses total protein loaded in each lane, and 2) the house-keeping gene GAPDH.

2.6.7. Statistical analysis

All data are expressed as mean ± standard deviation. Statistical significance was determined by one-way analysis of variance (ANOVA), followed by post hoc Tukey's test (except when stated otherwise). Significance was accepted at *p*-values inferior to 0.05.

3. Results and discussion

3.1. Adipose-derived extracellular matrix based electrospun bidimensional platforms

As long-established, the morphology of electrospun fibers stems from the integration of various factors such as solution viscosity and electrical conductivity as well as the spinning working parameters, particularly the applied voltage [41]. Primarily, factors such as collection distance, voltage and solution concentration were optimized to produce nano-sized bead-free fibers of a blend based on adECM and synthetic co-polymers of lactide/caprolactone. The influence of the adECM/copolymer ratio (60/40; 70/30 and 80/20) and the amount of lactide in the lactide/caprolactone copolymer (100, 85 and 70%) on the morphology, hydrophilicity and mechanical properties of the electrospun membranes are shown in Fig. 1. All formulations yield bidimensional nanofibrous platforms with smooth, bead and fusion-free fibers with most up to 900 nm in diameter. As the amount of lactide increases in the copolymers, the viscosities of the PLC copolymers (PLA70, PLA85) and the PLA100 increase from 1.5 to 1.6 and 1.8 g/mL, respectively, which accounts for a slight increase in the frequency of larger fibers (Fig. 1**a**), an effect inherent to viscosity in the electrospinning process [42]. Similarly, when increasing the adECM from 60 to 70%, the resulting viscosity of the composite solution decreases, thereby leading to a higher percentage of smaller fibers within the low range of 300 to 600 nm. Besides the viscosity factor, the adECM proteins may act as polyelectrolytes, raising the charge density on the solution surface and subsequently the electrical potential difference leading the jet to expel thinner fibers [43]. Similar observations were reported in binary systems of PLC/collagen [44] and PLC/gelatin [45] wherein fiber diameter gradually decreases upon the addition of gelatin and collagen. However, when further increasing adECM to 80%, the jet becomes unstable preventing thinner fibers to reach the collector, leading to a final membrane of lower thickness and more fibers with larger diameters.

Structural analysis via FTIR-ATR (Fig. 1**b**) illustrates the characteristic vibrational bands from the following bidimensional electrospun platforms: 2D adECM, 2D PLA70 and the blends with different ratios. The bands of 2D PLA70 are typically CH_2 and CH_3 stretching (3000–2800 cm^{-1}), C = O group stretching (1746 cm^{-1}), asymmetric CH bending (1454 cm^{-1}) and symmetric CH bending (1382 cm^{-1}) [46], while the electrospun 2D adECM spectrum shows the bands of Amide A (3200–3500 cm^{-1}), Amide I (1642 cm^{-1}), Amide II (1540 cm^{-1}) and Amide III (1218 cm^{-1}) [47]. When combined, the bidimensional electrospun blends basically followed the infrared characteristics of both constituents, wherein the characteristics bands of adECM are more intense as its content within the blend increases. Regarding their interplay, a slight shift of C = O (1746 to 1754 cm^{-1}) from 2D PLA70 and the NH stretching vibrations from the Amide A (3286 to 3280 cm^{-1}) suggests adECM interaction with the carbonyl of the poly (lactide-caprolactone), as observed elsewhere in collagen/PCL electrospun nanofibers [48].

As envisioned by the use of a high content of adECM in the electrospun blends, all bidimensional electrospun platforms are hydrophilic, with water contact angle (WCA) between 58 and 80° [49,50] (Fig. 1**c**), thus suitable for cell adhesion. Polylactide acid (PLA100) and its co-polymers with caprolactone (PLA85, PLA70) are hydrophobic in nature [45] and the addition of adECM endows the resulting nanofibrous membranes with an hydrophilic character, owing to the amino, carboxylic and hydroxyl polar groups found in its proteins [51]. The WCA was determined right after the drop entered in contact with the membranes surface since it was quickly absorbed by the platforms, displaying values around 0° just after 30 s. Besides the contribution of the chemical composition, the surface roughness and the variable fibre diameter can account for the slight differences in the measured WCA [50].

The most appreciable effect of incorporating caprolactone into the lactide/caprolactone copolymer on the adECM-based bidimensional platforms reflects on their mechanical properties (Fig. 1**d and 1e**). During tensile experiments, the 2D platforms exhibit the traditional stress–strain curve profile characterized by an initial elastic region, followed by the yield point and finally the strain-hardening region. By simply integrating 15 and 30% of caprolactone (PLA85 and PLA70), two valuable effects are achieved in the bidimensional platforms. Without significantly changing the hydrophilicity and surface chemistry, the tensile modulus can be modulated towards lower values (around 35 %) targeting the soft neural tissue. Additionally, owing to PCL elasticity, the copolymer behaves like an elastomer, conferring toughness, characterized by longer strain-hardening region [52]. Expectedly, the 2D blends produced with the highest content of adECM, i.e. adECM/PLA70 with a ratio of 80/20, presents the lowest value of tensile modulus (61.9 ± 4.8 MPa) owing to the contribution of its soft proteins.

3.2. Decellularized adipose-derived extracellular matrix based three-dimensional nanofibrous platforms

The 2D platforms were successfully converted into 3D nanofibrous platforms via gas foaming – expansion via immersion in $NaBH_4$ aqueous solution – resulting in a 3D continuous interconnected layered structure of nanofibers. The gas release from $NaBH_4$ dissolution in water penetrates in the interspace of the bidimensional platforms, allowing an accumulation of H_2 trapped inside pores that induces pressure on the surrounding fibers, resulting in the formation of the 3D structure [53]. After just one minute of immersion in 0.25 M $NaHB_4$ solution, the platforms expanded around 33-fold in the Z direction, along a slight decrease of width and length (Fig. 2**a**). While early studies on expanding PCL electrospun membranes by gas foaming reported low expansion capacity in 0.1 M of $NaHB_4$ and longer time of reaction [28], binary systems of PCL combined with natural proteins which are more hydrophilic, have demonstrated higher foaming capacity. For instance, when blended with silk fibroin, a 4 fold expansion was obtained in 20 min using 0.1 M $NaBH_4$ [53]. PVA/chitosan system also achieved high level of expansion (25 times the initial height) using concentrations of $NaHB_4$ superior to 0.1 M and/or immersion above 30 min [54]. The remarkable expansion achieved in this work is attributed to the adECM as a reflection of the intrinsic elasticity of its constituents such as elastin and collagen. The nature of the copolymer employed to blend with the adECM did not significantly change the expansion capacity (Fig. 2**c**). Regarding the adECM/PLA ratio, while increasing the adECM content from 60 to 70% also did not change the expansion magnitude, the membrane with 80 % of adECM expanded in a smaller extent. This is attributed to the higher frequency of larger fibers which offer more resistance to the H_2-induced pressure.

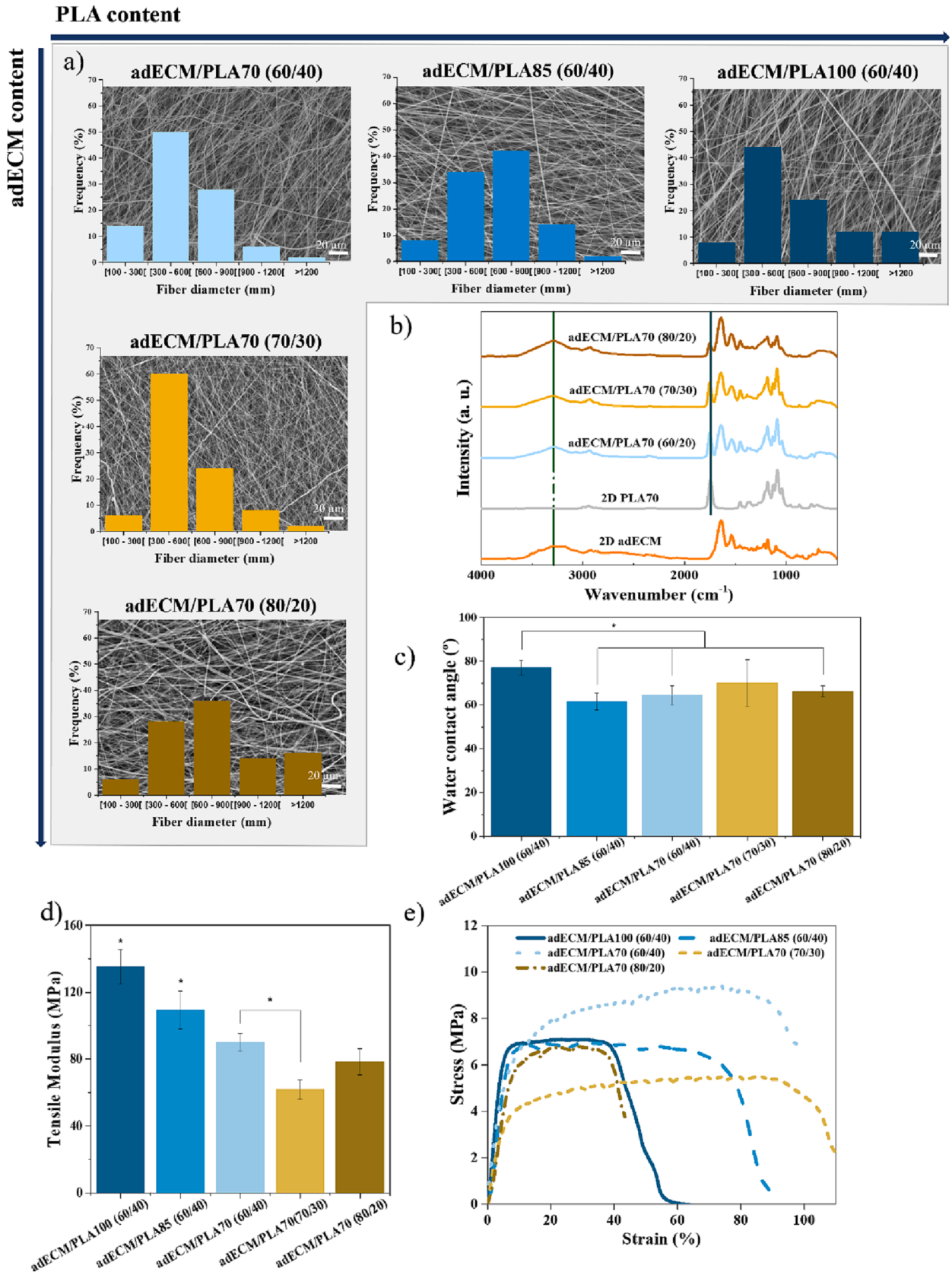

Fig. 1. Characterization of electrospun nanofibers depending on adECM and copolymer nature and ratio: a) Morphological analysis: SEM images and nanofiber diameter distribution (insets). Scale bar 20 µm; b) ATR-FTIR spectra; c) Water contact angles; d) Mechanical analysis specifically, tensile modulus and e) Stress–strain profile curves.

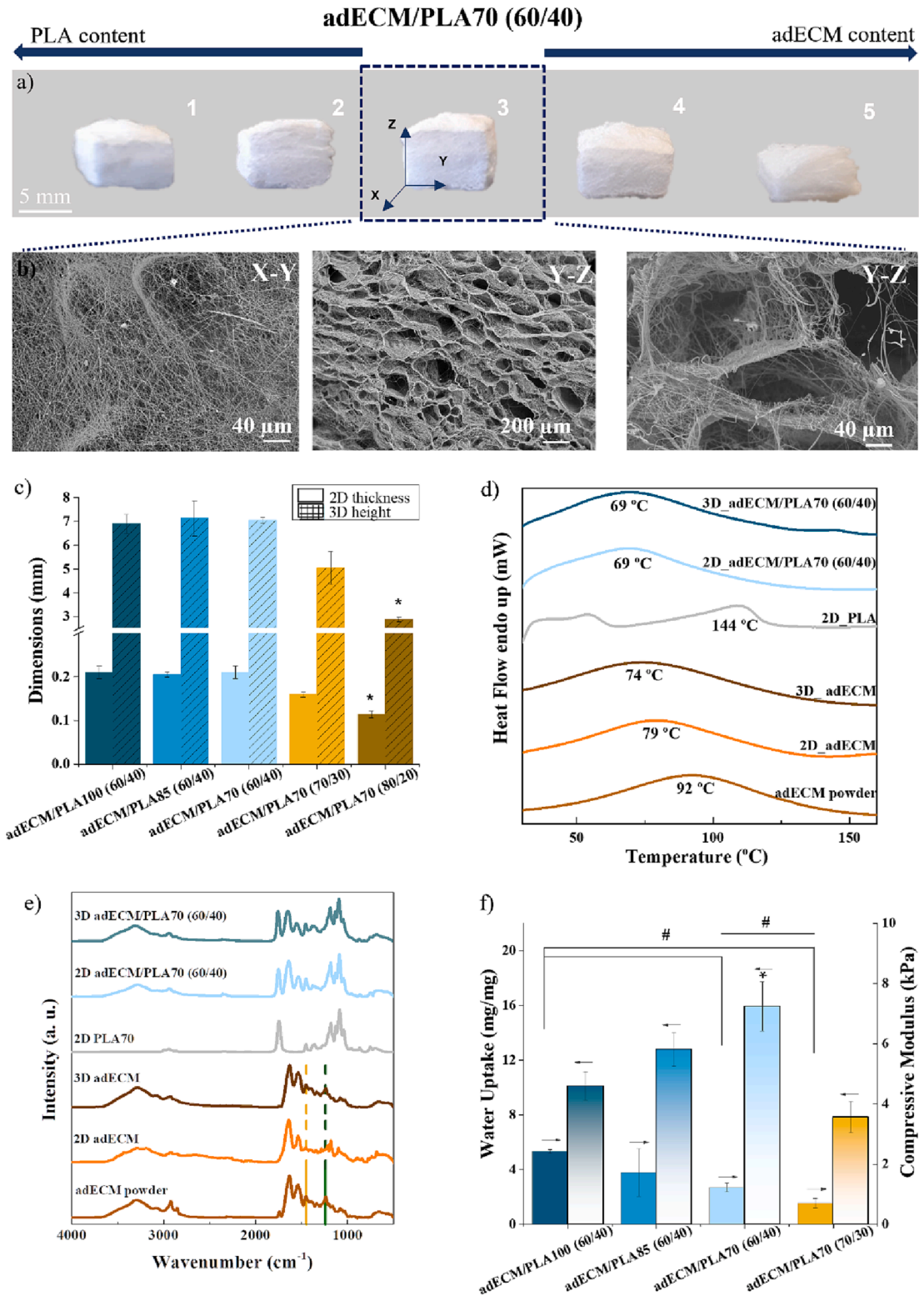

Fig. 2. A) Photographs of 3D platforms: 1-adECM/PLA100 (60/40), 2- adECM/PLA85 (60/40), 3- adECM/PLA70 (60/40), 4- adECM/PLA70 (70/30) and 5- adECM/PLA70 (80/20); b) SEM images of 3D adECM/PLA70 (60/40) platform: XY plan; YZ and magnification of YZ plan; c) thickness of the 2D membranes and expansion after gas foaming; d) DSC thermograms; e) ATR-FTIR spectra; f) Water uptake and Compressive Young's modulus. Statistical analysis by One-way ANOVA followed by post hoc Tukey test: $^{*}p < 0.05$, $^{\#}p < 0.05$, where * denotes statistically significant differences between platforms while #, in graph f), denotes statistically significant differences in the compressive young modulus of the different platforms.

Structurally, the faces corresponding to XZ and YZ planes display intercalated layers of nanofiber arrays and gaps (Fig. 2**b**). The interlayer spacing is in the range of 25–500 μm, which is a favorable microenvironment for cell diffusion and proliferation [55]. On the other hand, the top and bottom surfaces, XY planes, are denser arrangements of fibers without large pores, resembling the original bidimensional membranes.

While a 2D nanofibrous membrane was electrospun solely from an adECM solution to obtain additional information on the implications of processing the adECM via electrospinning and subsequent gas foaming on its biochemical integrity, the resulting 3D platform was deemed unsuitable as it partially collapsed due to proteins reorganization upon hydration in PBS. Blending with the copolymer provides structural stability after the gas foaming process.

Shaping proteins into three-dimensional scaffolds bears several challenges such as protecting and retaining their biochemical features for optimal bioactivity *in vitro* and *in vivo*. This aspect is sometimes overlooked while pursuing specific morphological and physical properties of 3D constructs. Literature cautions on substantial less stability even on commercial scaffolds based on various ECM due to various degrees of processing-induced destabilization in relation to the their respective source tissue [56]. Many factors in electrospinning collagen such as employing fluoroalcohols and electric field may be responsible for low to high degree of protein denaturation [57]. Here, DSC and FTIR analyses (Fig. 2**d and 2e**) provide insights on the effect that successive processing had on the adECM organization. The thermal denaturation profile of adECM-based products translates not only the stability of its individual constitutive proteins, but also the complex supramolecular assembly of these elements in terms of fibrogenesis, nanofiber and microfiber formation capacity and their alignment, as well as the deposition and interaction of the non-collagenous compounds. Transforming adECM powder into adECM-based nanofibers via electrospinning, which encompassed adECM digestion, dissolution and application of an electric field led to some degree of structural destabilization. Indeed, the broad endothermic peak at 92 °C observed for the adECM powder decreased to 79 °C for the adECM electrospun membrane (2D adECM), implying that less energy is required to unfold and denature the adECM compounds (Fig. 2**d**). The effect of this structural destabilization of the adECM was investigated on the metabolic activity of NSCs (Figure S4) and revealed that although it induced lower metabolic activity, it did not severely compromised the proliferative ability of the cultured cells.

When further compositing adECM with the copolymer, the thermal denaturation temperature of the bidimensional adECM/PLA70 nanofibrous platforms diminishes further about 10 °C. In the collagen organization, the triple helices interact via hydrogen bonds and self-assemble into highly organized and hierarchical microfibrillar structures. The incorporation of the copolymer chains, owing to the interaction of their carbonyl bond with the amide A, interferes in the supramolecular interactions between adjacent triple helices by disrupting hydrogen bonds, leading to a less ordered self-assembling of the triple helices.

After converting the 2D electrospun membrane into a 3D nanofibrous construct, the denaturation temperature did not vary, thereby suggesting that the gas foaming process, which includes pressure from the gas on the nanofibers followed by rinsing and short freeze-drying, did not further alter the adECM protein organization in relation to the prior alteration caused by the addition of the copolymer. However, when electrospinning adECM only and subjecting the resulting membrane to gas foaming, a slight decrease in thermal stability is observed - from to 79 to 74 °C, suggesting that the organizational variation induced by the copolymer prevent further disorganization upon the gas foaming process. In fact, when immersing the adECM nanofibrous membrane into the sodium borohydride solution, the hydrated collagen fibrils are subjected to the gas-induced pressure that may cause expansion of their intrafibrillar space. Additionally, gas foaming is followed by freeze-drying that has potential for a slight destabilization of collagen fibrils due to the imposed mechanical stress by ice formation [58,59]. Thus, the intermolecular hydrogen interactions provided by the copolymer restrict further motion of the collagen molecules and prevent supplemental disorganization when applying the gas-foaming process, that emerges as an attractive and easy process to convert adECM based bidimensional hybrids into three-dimensional nanofibrous architectures. Noteworthy, the variation in the adECM thermal stability induced by the combination of electrospinning and gas foaming is not larger than the one observed in traditional freeze-dried and crosslinked adECM-based scaffolds (**Figure S1**).

In FTIR spectra (Fig. 2**e**), Amide I is detected at different wavenumbers according to the secondary structure of the protein, so it is commonly used as a reference to infer protein denaturation [52]. Infrared spectroscopy revealed a slight shift when electrospinning adECM (6 to 8 cm^{-1}), regardless if blended or not with the copolymer PLA70. Expectedly, the combined use of organic solvents and electric field may have caused some degree of denaturation, corroborating the DSC analysis that pointed to the presence of unfolded structures. Gas foaming did not induce further shift on the Amide I, while it did alter the position of Amide A and Amide II towards higher wavenumbers. Notwithstanding the presence of unfolded structures that relate to partial denaturation of the protein, the collagen triple helices can retain their structural integrity. This can be probed by the ratio between peaks around 1240 cm^{-1} (amide III) and 1450 cm^{-1}, wherein values around 1 are indicative of a triple helical structure and values around 0.5 suggests protein denaturation [60]. Here, a slight decrease from 0.97 for the adECM powder to 0.85 for the gas foamed adECM platforms implies that, whereas some unfolding of adECM components have occurred, the triple helices have preserved their structural integrity. While a partial loss of biological and structural integrity may be of concern, both *in vitro* and *in vivo* evidence have shown that electrospun collagen improved healing in dermal and muscle reconstruction compared to electrospun gelatin so-that the exact collagen native structure does not require a strict replication to take advantage of its biological activity. In fact, both native and denatured collagen α chains, independently from their arrangement, have shown distinctive biological properties, that outperforms electrospun gelatin [61].

The 3D platforms were submitted to PBS uptake measurements and mechanical compression to evaluate their adequacy as scaffolding strategies for the central nervous system, specifically the spinal cord tissue (Fig. 2**f**). All 3D platforms presented low Young's modulus ranging from 1.55 to 5.33 kPa. The continuous, porous, and layered elastic structure of the adECM/copolymer conferred the platforms the ability to return to their initial shape in seconds, allowing an easy manipulation (video S1). In contrast to other tissues, the SCI has a specific pathophysiology including secondary injury mechanisms that can be particularly detrimental to tissue repair. Namely, fibroblasts infiltrate the lesion and form a scar fibrous tissue. If the scaffold is too soft, it may suffer from the tissue contraction *in vivo*, due to the pathophysiological fibrous tissue formation induced by fibroblasts invading the lesion during the secondary injury [62]. Strategies based solely on decellularized extracellular matrices have sometimes poor performance after implantation due to a structural collapse following fibrosis at the lesion site [7]. Here, the copolymer imparted structural stability to the ECM-based 3D platforms. Interestingly, electrospun nanofibrous PLGA used as shell for an ECM freeze-dried scaffold demonstrated *in vivo* to serve as an effective barrier to isolate the infiltration of meningeal fibroblasts, providing a milieu with less fibrotic invasion [7]. Similarly, it is envisaged that the denser peripheral layers of the gas foamed 3D construct can be beneficial for physically segregating the infiltrating fibroblasts from the surrounding connective tissue. Mechanical compliance is another critical factor for an appropriate integration of the scaffold. The adECM/PLA70 (60/40) formulation was characterized by a Young's modulus of 1.55 ± 0.36 kPa, as low as soft rGO aerogels (1.3 ± 1.0 kPa) that reportedly demonstrated mechanical compliance towards neural cells and spinal cord tissue and enhanced the reparative neural responses in chronic hemisected spinal cord in rats, by avoiding scar retraction within the lesion site while allowing axons to grow [63].

Beyond the biomimicry intent, using nanofibers as building blocks for three-dimensional scaffolds also preclude the critical issue of cell loss or neuropathy that can be induced by non-physiological local stress [19]. While all 3D platforms exhibited a high PBS uptake capacity, saturating after just one hour, the adECM/PLA70 (60/40) formulation presented the highest uptake, resulting from the complex synergy between the hydrophilicity of the adECM components, the fibers surface wetting properties and the interfiber pore volume across the nanofibrous network.

3.3. Incorporation of PDA-rGO in the bidimensional and three-dimensional adECM-based nanofibrous platforms

PDA-rGO was successfully synthesized according to a method previously reported in the literature. ATR-FTIR, XRD and Raman spectroscopies were used to monitor the reduction process (**Figure S2** and discussion in supplementary information (SI)). Based on its suitable set of structural properties, the formulation adECM/PLA70 (60/40) was selected to incorporate 1.5 % (w/w) of PDA-functionalized rGO, henceforward named adECM/PLA and adECM/PLA PDA-rGO. Similarly, to its undoped counterpart, adECM/PLA PDA-rGO was electrospun into a dense arrangement of uniform and bead-free nanofibers, with PDA-rGO sheets homogeneously integrated onto the membrane (Fig. 3**a**). The average fiber diameter decreased from 564 ± 238 nm to 377 ± 158 nm in undoped and PDA-rGO doped samples respectively, presumably due to the improved conductivity of the electrospinnable solution (Fig. 3**b**). Furthermore, when transforming the 2D electrospun membranes into the 3D constructs, the pore size distribution of the PDA-rGO doped ones shifted slightly towards higher pore sizes (Fig. 3**e and 3f**), attributed to the repulsion between rGO sheets, previously observed in 3D self-assembled rGO sheets and PCL-gelatin nanofibers [25]. Besides this discrete morphological variation with regard to the 2D nanofibrous platforms and their 3D analogues, the low loading of PDA-rGO was not sufficient to promote significant alterations in the wettability and tensile modulus of the bidimensional platforms (Fig. 3**c and 3d**). Parallelly, the fluid uptake capacity and the compressive modulus of the respective 3D undoped and PDA-rGO doped platforms were also similar (Fig. 3**g and 3h**). Thus, since the main structural properties are not significantly altered by the polydopamine-functionalized rGO doping, its potential effect on the NSCs can be easily singled out. Noteworthy, a homogenous distribution of PDA-rGO across the 3D nanofibrous construct is clearly visible owing to the uniform grey appearance imparted by the PDA-rGO (photographs of 3D nanofibrous constructs in **Figure S3**).

Neurite outgrowth as well as axonal elongation are critical for the

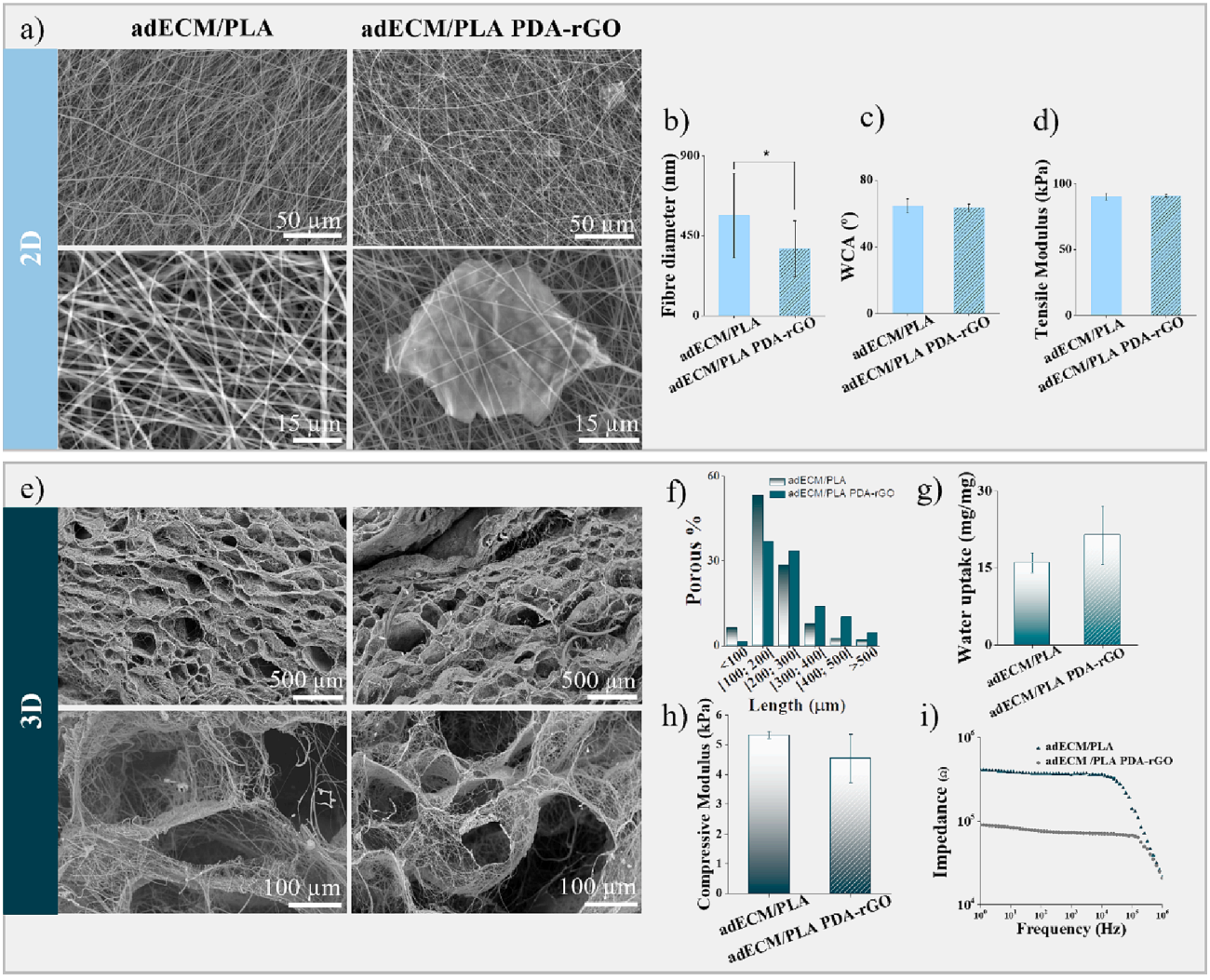

Fig. 3. Characterization of the bidimensional and three-dimensional platforms based on the formulation adECM/PLA70 (60/40) and its composites with PDA-rGO denoted here as 2D adECM/PLA, 2D adECM/PLA PDA-rGO, 3D adECM/PLA and 3D adECM/PLA PDA-rGO: a) SEM images of the 2D platforms; b) Fiber diameter; c) Water contact angle; d) Tensile modulus; e) SEM images of the 3D platforms; f) Pore size distribution; g) Water uptake; h) Compressive modulus; and i) EIS measurements log(|impedance|) vs log(frequency). Statistical analysis by One-way ANOVA (*denotes statistical difference $p < 0.05$).

formation of neuronal circuits required in neural tissue repair. Besides guiding neurite outgrowth by physical cues, electrical stimulation can also direct it. Electrical conductivity was evaluated to determine if doping the adECM-based platforms with polydopamine-functionalized rGO had a significant effect. Depending on the stimulating frequency, the resistance of the platform varies (Fig. 3**i**). For stimulating NSCs, the frequency parameter can be as low as 0.5 Hz for regeneration purposes and as high as hundred thousand Hz for deep brain stimulation [64,65]. The 3D nanofibrous platforms show a flat impedance profile for lower frequencies, while high frequencies get progressively less resistive. Conductivity was calculated for two of the most used frequencies in neural stimulation, 100 and 1 kHz. Deionized water was used because of its lower content of dissolved ions, thereby avoiding the contribution of ionic currents and for a better understanding of the intrinsic properties of the highly porous and nanofibrous 3D platforms. Doping the platforms with 1.5% (w/w) of PDA-rGO increased the electrical conductivity from $5.5x10^{-6}$ to $2.3x10^{-5}$ S/cm. This further supports the observation of a homogeneous distribution of PDA-rGO across the nanofibrous construct. The conductivity of the PDA-rGO containing 3D platform was predictably lower than the one obtained in bidimensional electrospun silk fibroin/poly(l-lactic acid-co-caprolactone) with 4 coatings of rGO ($4 x10^{-4}$ S/cm) [66], owing to its highly porous network comparing to a dense electrospun membrane. Still, a significant conductivity improvement is evident in the rGO-doped platforms, from a low slope region of 400–300 kΩ to 100–50 kΩ. With lower impedance platforms, current can flow and interact with cells in the surroundings.

3.4. *adECM-based 2D and 3D platforms for NSCs migration, proliferation and differentiation*

Embryonic stem cells are tissue-specific pluripotent cells, that divide to generate progenitor cells, which further differentiate into fully functional terminally differentiated cells. While the supply of human cells is limited and raises ethical concerns, murine cells represent an advantageous alternative since they are genetically similar to human cells [67] and are readily available. A commercial immortalized murine cell line was employed as a suitable alternative to human cells to screen the cytocompatibility of the adECM-based bidimensional and three-dimensional nanofibrous platforms and analyze the effect of the morphology on the cells fate. NE-4C (CRL-2925 ATTC) is a NSC line isolated from cerebral vesicles of 9-day-old mouse embryo lacking functional p54 genes, with the ability to differentiate into either neurons or astrocytes when exposed to RA.

The NSCs display the usual clustered morphology with round-shaped

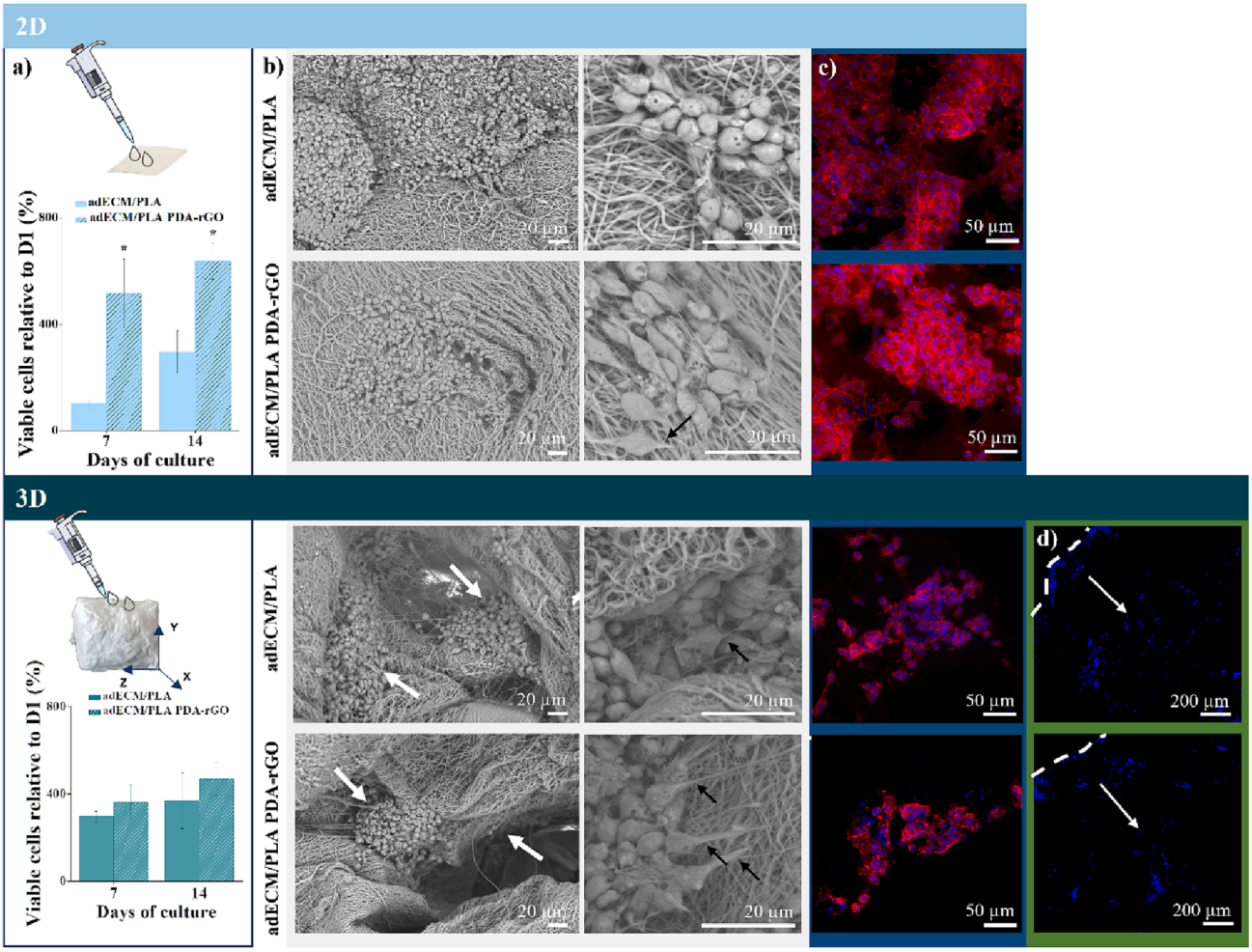

Fig. 4. Proliferation and morphology of NSC-seeded bidimensional and three-dimensional platforms: (a) Percentage of viable NSCs on the platforms relative to the adhered cells on day 1 after 7 and 14 days of culture and schematic illustrations of the seeding process in each platform; (b) SEM images of the NSC-seeded platforms after 7 days of culture, with white arrows highlighting the cellular clusters and black arrows pointing to the out-growing processes; (c) Immunocytochemistry of actin filaments (phalloidin in red) and nuclei (DAPI in blue) of the NSC-seeded platforms after 14 days of culture; (d) DAPI staining of the cross-sectioned NSC-seeded three-dimensional platforms, with white arrows showing the cellular migration pathway. Statistical analysis by One-way ANOVA followed by post hoc Tukey test: *$p < 0.05$, where * denotes statistically significant differences between platforms. (For interpretation of the references to colour in this figure legend, the reader is referred to the web version of this article.)

cells, characteristic from undifferentiated cells, well visible after 7 days (Fig. 4**b**) and further growing into confluency after 14 days in the bidimensional platforms as depicted in the phalloidin/DAPI staining (Fig. 4**c**). Since the three-dimensional platforms have virtually more than 2 orders of magnitude the available surface area, cells did not to reach confluency at day 14. Importantly, the interconnected microporosity - induced by the gas foaming process - effectively allows the migration of NSCs, as shown by DAPI-stained cells along the Y axis of the 3D platforms (Fig. 4**d**). Throughout the 3D constructs, the adECM cell-recognizable sites shaped into the nanofibrous pore walls act as anchoring niches for NSCs to adhere and grow, wherein large cell clusters are harbored (Fig. 4**b**, white arrows). When peeling off the dense peripheral layer of nanofibers in the 3D constructs, cell colonies were found up to 280 μm in thickness covering large areas of the nanofibrous internal walls. An enhanced cell infiltration *in vivo* has been linked to an increased density of regenerated axons [21], and is considered a primary condition to form sufficient endogenous neural relays within the short repair window after an acute injury [68]. Proliferation profile was assessed via a resazurin assay, an indicator of metabolic activity (Fig. 4**a**). In the bidimensional platforms, the presence of PDA-rGO greatly increased the metabolic activity of the NSCs. Similar behaviour was observed with a neuroblastoma cell line grown on bidimensional electrospun silk scaffolds, where as little as 1% of rGO enhanced the metabolic activity and proliferation of cells [69]. In contrast, PDA-

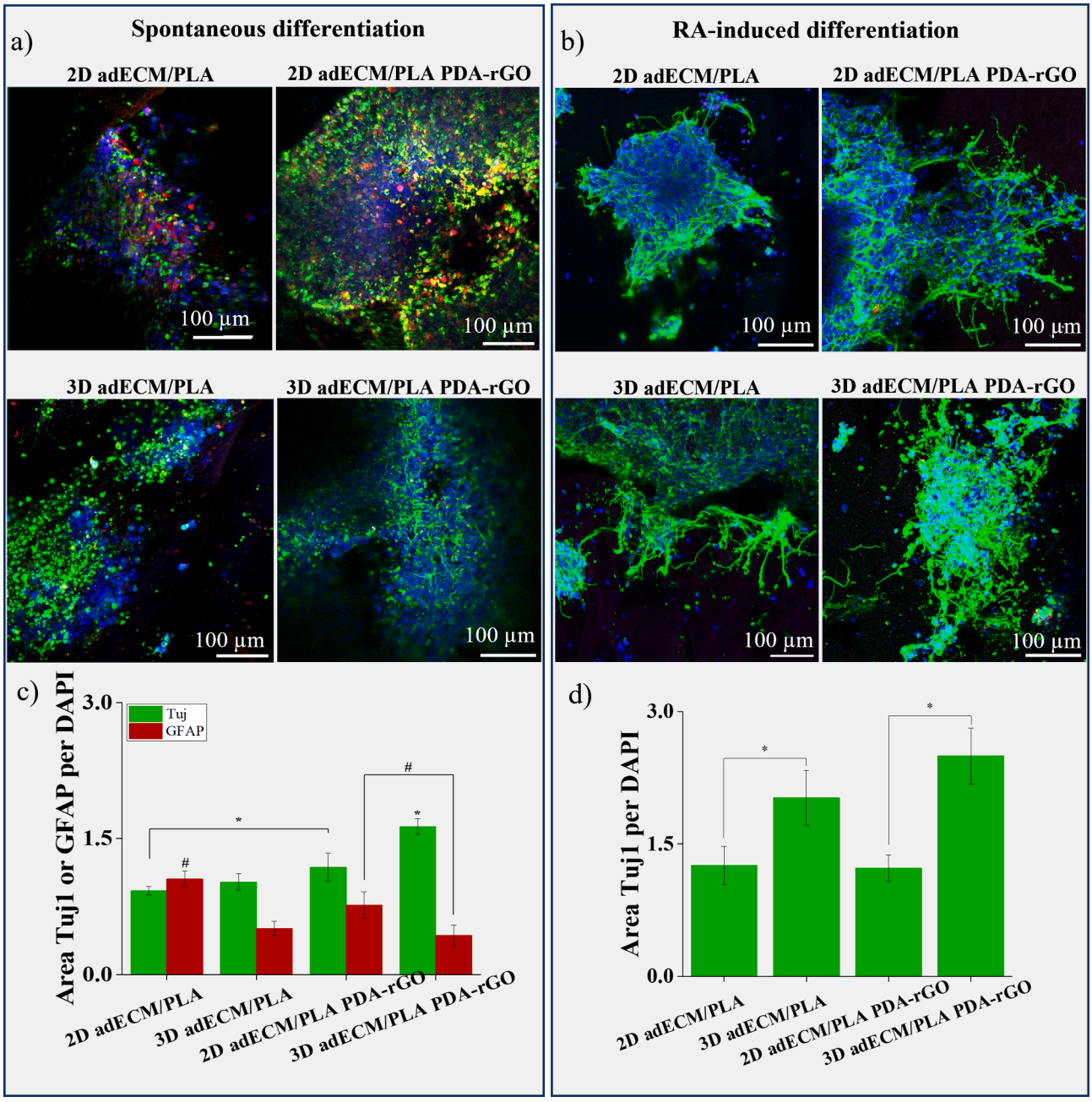

Fig. 5. NSCs spontaneous (a) and RA-induced (b) differentiation on bidimensional and three-dimensional platforms through immunocytochemistry of neuronal (Tuj1 in green) and astrocyte markers (GFAP in red) and cell nuclei (DAPI in blue) after 14 days culture. Quantification of the area covered by Tuj1 and GFAP per DAPI on spontaneous differentiation (c) and Tuj1 per DAPI on the RA-induced differentiation (d). Statistical analysis by One-way ANOVA followed by post hoc Tukey test: $^{*}p < 0.05$, $^{\#}p < 0.05$, where * denotes statistically significant differences between Tuj1-positive areas of the different platforms, while # denotes statistically significant differences between GFAP-positive areas of the different platforms. (For interpretation of the references to colour in this figure legend, the reader is referred to the web version of this article.)

functionalized rGO had no boosting effect on the metabolic activity of cells when grown onto the 3D platforms. This may be related to multiple factors. In fact, in 3D environments, the spatial distribution of integrin-mediated adhesions is largely different than in 2D, which affects cell spreading and subsequently impacts cell proliferation [70]. Also, the lower increases in metabolic activity within the 3D are potentially related to an onset of differentiation. Indeed, the cell morphology is appreciably different, with noticeable out-growing cellular processes attaching to the nanofibrous walls and projecting towards other cell clusters, particularly evident on rGO containing platforms (black arrows in Fig. 4**b**).

NSCs differentiation-related events, particularly lineage commitment and neuritogenesis, were investigated in two distinct conditions (Fig. 5). The first approach was to test the potential of the investigated platforms to affect spontaneous NSC differentiation in terms of lineage commitment, while the second relied on neuronal differentiating conditions commonly employed for NSC cultures, aiming to test the effects of the platforms in the neuritogenesis of NSC-derived neurons. In the neuronal differentiation conditions, retinoic acid was first used, followed by serum depletion and concomitant medium supplementation with BDNF - a growth factor involved in neuronal development and regeneration. In both scenarios, the platforms were immunolabeled for β-tubulin III (Tuj1), the tubulin isoform of neurons, present in their cell bodies and neurites (dendrites and axons), and a commonly used marker of immature neurons [71]. Further, since Tuj1 is also expressed by fetal astrocytes [72], cells on platforms were also labelled for glial fibrillary acidic protein (GFAP), a specific astrocyte cytoskeletal marker. Their expression was evaluated by quantifying the positive staining area of both Tuj1 and GFAP in microphotographs, normalized to DAPI area, depending on the architecture – 2D versus 3D – and the biochemical cue – only adECM-based versus adECM combined with PDA-rGO.

In the absence of differentiation-inductive factors, specifically no exposure to RA and BDNF, concurrently with maintaining the serum-supplemented medium, NCS clusters of mostly undifferentiated and immature early differentiated cells populate both two- and three-dimensional platforms. Undifferentiated cells are only stained with DAPI, while the later cells demonstrated individual immunoreactivity for Tuj1 (immature neurons) or dual immunoreactivity for GFAP and Tuj1 (immature astrocytes), and none or few neuritic projections (Fig. 5**a**). The fate of NSC was evaluated by quantifying the relative expression of the neuronal (Tuj1) and astrocytic (GFAP) markers (Fig. 5**c**). Interestingly, when the nanofibrous membranes are shaped into a 3D fibrous microenvironment, commitment towards the astrocytic lineage seems to be significantly prevented, illustrated by less GFAP (red) staining observed via confocal imaging and significant less GFAP/DAPI area. Furthermore, the incorporation of a little amount of rGO boosts the differentiation towards the neuronal lineage, both in the 2D membranes and the 3D nanofibrous platforms, given the concomitant increase in the Tuj1/DAPI area and decrease in the GFAP/DAPI area for platforms with PDA-rGO. Also, consonant with culture conditions not inducing differentiation, neuritogenesis is absent except for the 3D constructs doped with PDA-rGO, which exhibit emerging neurites within the cell clusters (and a concomitant Tuj1/DAPI area greater than 1.0). The results thus indicate that adECM-based nanofibers, organized in a 3D environment and combined with the biomimetic-inspired rGO, induce spontaneous differentiation of NSC toward neurons. These findings are in accordance with the growing evidence found in literature on the ability of rGO to promote the phenotypic determination of neural cells independently of how rGO is exploited - as a standalone scaffold or an additive. In three-dimensional self-assembly of rGO sheets and PCL-gelatin nanofibers, the partially reduced rGO triggered the best neural progenitor cell response.[25] A simple coating of rGO on a porcine-derived dermal matrix also demonstrated to induce the neuronal differentiation of bone-marrow-derived MSC [73]. The accelerated differentiation by rGO has been linked to a few mechanisms such as its high capability for electron transfer and ability to affect mechanotransduction [74]. Parallelly, polydopamine-functionalized substrates have shown to enhance differentiation of human NSCs at a level comparable or greater than Matrigel®, owing to polydopamine ability to efficiently immobilize growth factors, adhesion peptides and other molecules favourable to neural development [75].

When using neuronal differentiation-inducing conditions for the NSCs culture (Fig. 5**b**), as expected, a high number of NSC appreciably develop a neuronal morphology and present extensive neuritogenesis, shaped into a dense branching of long processes extending out of the neuronal cell bodies. This dense neuritic network is apparent within the cells clusters as well as branching out of them. Axonal growth depends on contact-mediated cues which can be provided by both the adECM-based nanofibers and PDA-functionalized rGO, and diffusible cues expressed by neighboring cells or found in the medium. Since neural cell clusters are chemotactic microenvironments, wherein diffusible cues from the medium are more concentrated at the periphery, thicker neurite outgrowth is more evident at the cluster periphery (**Figure S5**). Accordingly, the quantification of the immunolabeling reveals high levels of Tuj1 expression (Fig. 5**d**) while the GFAP staining remains negligible (not shown). Furthermore, more intricate and denser neuritic networks, critical for the maturation of the neuronal culture [76], are formed within the neuronal cell clusters in the three-dimensional constructs. Thus, when using RA combined with BDNF supplementation at day 6 and 8 of culture, the NSC fate commitment was efficiently driven towards neuronal differentiation, particularly within the three-dimensional constructs. This is expected, since RA is an early differentiation trigger, that starts mediating early neurite outgrowth and increases the expression of neurotrophic receptors such as TrkB (the main BDNF receptor) [76,77], while BDNF supplementation boosts the neuronal differentiation program, including neuritic elongation.[77].

Under these pro-neuronal cultures, the differentiation effect of the mediated-contact PDA-rGO cue is overshadowed by the strong chemical and diffusible cues provided by the RA acting synergistically with BDNF. While RA is a differentiation inductor, it also mediates neurite outgrowth by regulating the expression of the transcription of neurotrophic receptors such as BDNF [76]. BDNF direct supplementation further supports neurite outgrowth [78]. Noteworthy, while the effect of PDA-rGO becomes statistically non-significant, the 3D spatial arrangement of the nanofibers – induced by the gas foaming - have a remarkable effect on the phenotype determination and the neurite formation. This result reinforces the critical importance of engineering scaffolds with multiple length-scale architecture. On the other hand, in this analysis of microphotographs, the differentiation effect of the mediated-contact PDA-rGO cue is still apparent, but statistically non-significant when compared to the 3D adECM/PLA. To further understand if the PDA-rGO cue can improve neuronal differentiation and/or neuritogenesis in a 3D spatial arrangement, immunoblot analyses of the protein levels of Tuj1 and MAP2 'a' and 'b' isoforms of higher molecular weight, widely used neuronal markers [79], were performed (Fig. 6). Both Tuj1 and MAP2a/b levels significantly increase by ~ 1.26-fold and ~ 1.72-fold, respectively, in NSCs grown on 3D adECM/PLA PDA-rGO under neuronal differentiation conditions, relatively to 3D platforms without PDA-rGO. Tuj1 protein levels are well known to increase throughout the course of neuronal differentiation, alongside with the increase in neuritic length [80]. Further, during neuronal differentiation the expression of the MAP2 'a' and 'b' neuronal isoforms increase (while the expression of other more ubiquitous MAP2 isoforms of lower molecular weight decrease, **Figure S6**), with MAP2b being required for neurite outgrowth/extension and MAP2a being associated with the maturation of dendrites, including their increased thickness [81-83]. These results are aligned with the previous observation that the PDA-rGO cue promotes differentiation towards the neuronal lineage and/or neuritogenesis. Based on the promising results, before implantation in a SCI animal model, further evaluation should include assays within ISO 10993 concerning the biological evaluation of medical devices. Specifically, assays respective to hemocompatibility, genotoxicity and

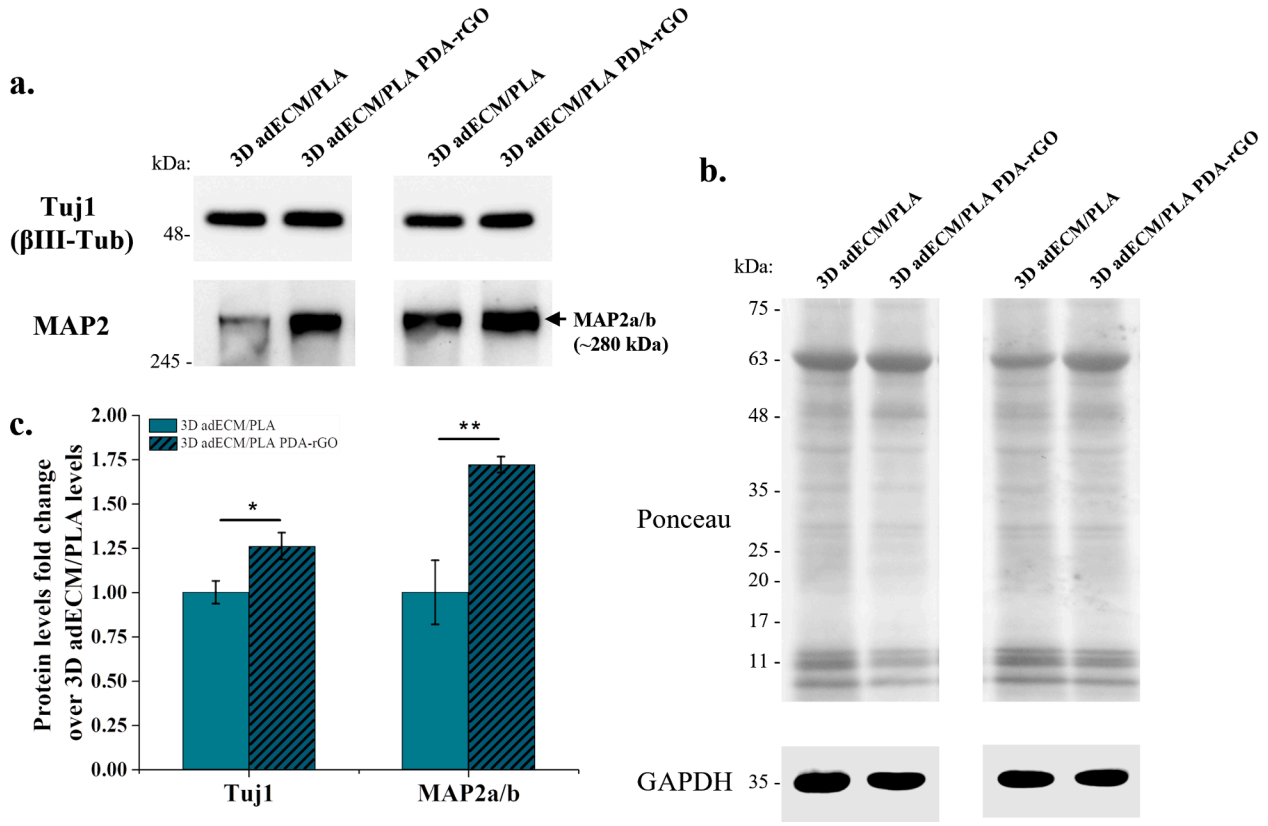

Fig. 6. Immunoblot analysis of the protein levels of Tuj1 (alias βIII-tubulin) and MAP2a/b neuronal isoforms (of higher molecular weight, ~280 kDa), in lysates of NSCs grown for 14 days on 3D adECM/PLA and 3D adECM/PLA PDA-rGO, under RA + BDNF neuronal differentiation conditions (a); Densitometric quantifications of the protein bands were corrected to the relative quantifications of two loading controls: Ponceau S staining and the housekeeping gene GAPDH (b); Molecular weight markers are indicated to the left (a and b). Relative quantification of the fold changes in protein levels of Tuj1 and MAP2a/b, expressed as the ratio of their levels in cells grown on 3D adECM/PLA PDA-rGO relative to the ones on 3D adECM/PLA, taken as 1.0 (c). Statistical analysis by two-tailed unpaired T-test: $*p < 0.05$, $**p < 0.01$.

identification/quantification of degradation products and their systemic effect *in vivo* will be conducted.

4. Conclusion

Here, an adipose-derived decellularized extracellular matrix, assisted by a lactide-caprolactone copolymer, is shaped into a three-dimensional nanofibrous microenvironment by electrospinning combined with gas foaming. Optimizing the proportion of the copolymer in relation to the decellularized extracellular matrix as well as varying the caprolactone content in the copolymer led to a fine tune of the 3D nanofibrous constructs, that exhibit structural stability, adequate microporosity and mechanical compliance with soft neural tissue such as the spinal cord.

Taken together, the 3D nanofibrous architecture and unique biochemical features of the adECM provided microenvironmental cues to guide neural stem cells adhesion and migration. Furthermore, the adECM-based platforms were doped with polydopamine functionalized rGO to boost their performance as platforms to direct stem cell fate and neuritogenesis.

The metabolic activity/proliferation of neural stem cells was highly dependent on rGO presence on bidimensional platforms while not visibly affected when grown into the three-dimensional platforms. Regarding NSC differentiation, in the absence of exogenous diffusible signaling that drives differentiation (i.e. RA and BDNF), the results suggest that polydopamine-functionalized rGO encourages the stem cells spontaneous differentiation toward the neuronal lineage, in both 2D and 3D platforms. Under well-established pro-neuronal differentiation conditions, the 3D platforms were the most favorable to promote the acquisition of a neuronal phenotype. More specifically in the 3D platforms, PDA-rGO further boosts neuronal differentiation, translated by an increase of 1.26-fold and 1.72-fold in the levels of Tuj1 and MAP2a/b neuronal isoforms, respectively. Thus, although broadly exploited, electrospun membranes are hardly effective platforms to test neural stem cells response in a physiological-like environment. Gas foaming is a straightforward technique to produce 3D nanofibrous constructs with tunable properties, so-that when testing novel biomaterials, it readily provides a 3D microenvironment, that reveals biomaterial-induced effects which otherwise could remain unperceived.

Declaration of Competing Interest

The authors declare that they have no known competing financial interests or personal relationships that could have appeared to influence the work reported in this paper.

Data availability

Data will be made available on request.

Acknowledgements

This work was supported by the European Union's Horizon 2020 research and innovation programme under grant agreement No 829060 (FETOPEN project: NeuroStimSpinal), and the Portuguese following funding: UIDB/00481/2020 and UIDP/00481/2020, iBiMED (UIDB/4501/2020 and UIDP/4501/2020), the LiM Bioimaging Facility (a PPBI node, POCI-01-0145-FEDER-022122) - Fundação para a Ciência e a

Tecnologia (FCT) and CENTRO-01-0145-FEDER-022083 - Centro Portugal Regional Operational Programme (Centro2020) under the PORTUGAL 2020 Partnership Agreement, through the European Regional Development Fund. B.M.S. acknowledges financial support from FCT through the doctoral scholarship 2020.06525.BD.

Appendix A. Supplementary data

Supplementary data to this article can be found online at https://doi.org/10.1016/j.cej.2023.144980.

References

[1] C.S. Barros, S.J. Franco, U. Müller, Extracellular Matrix: Functions in the nervous system, Cold Spring Harb. Perspect. Biol. 3 (2011) 1–24, https://doi.org/10.1101/cshperspect.a005108.

[2] A.E. Haggerty, M.M. Marlow, M. Oudega, Extracellular matrix components as therapeutics for spinal cord injury, Neurosci. Lett. 652 (2017) 50–55, https://doi.org/10.1016/j.neulet.2016.09.053.

[3] E. Garreta, R. Oria, C. Tarantino, M. Pla-Roca, P. Prado, F. Fernández-Avilés, J. M. Campistol, J. Samitier, N. Montserrat, Tissue engineering by decellularization and 3D bioprinting, Mater. Today. 20 (2017) 166–178, https://doi.org/10.1016/j.mattod.2016.12.005.

[4] Z. Kočí, K. Výborný, J. Dubišová, I. Vacková, A. Jäger, O. Lunov, K. Jiráková, Š. Kubinová, Extracellular Matrix Hydrogel Derived from Human Umbilical Cord as a Scaffold for Neural Tissue Repair and Its Comparison with Extracellular Matrix from Porcine Tissues, Tissue Eng. Part C, Methods. 23 (2017) 333–345, https://doi.org/10.1089/ten.tec.2017.0089.

[5] J.Y. Hong, Y. Seo, G. Davaa, H.-W. Kim, S.H. Kim, J.K. Hyun, Decellularized brain matrix enhances macrophage polarization and functional improvements in rat spinal cord injury, Acta Biomater. 101 (2020) 357–371, https://doi.org/10.1016/j.actbio.2019.11.012.

[6] J.-H. Sun, G. Li, T.-T. Wu, Z.-J. Lin, J.-L. Zou, L.-J. Huang, H.-Y. Xu, J.-H. Wang, Y.-H. Ma, Y.-S. Zeng, Decellularization optimizes the inhibitory microenvironment of the optic nerve to support neurite growth, Biomaterials. 258 (2020), 120289, https://doi.org/10.1016/j.biomaterials.2020.120289.

[7] Y. Ma, H. Shi, Q. Wei, Q. Deng, J. Sun, Z. Liu, B. Lai, G. Li, Y. Ding, W. Niu, Y. Zeng, X. Zeng, Developing a mechanically matched decellularized spinal cord scaffold for the in situ matrix-based neural repair of spinal cord injury, Biomaterials. 279 (2021), 121192, https://doi.org/10.1016/j.biomaterials.2021.121192.

[8] M. Cicuéndez, L. Casarrubios, M.J. Feito, I. Madarieta, N. Garcia-Urkia, O. Murua, B. Olalde, N. Briz, R. Diez-Orejas, M.T. Portolés, Effects of Human and Porcine Adipose Extracellular Matrices Decellularized by Enzymatic or Chemical Methods on Macrophage Polarization and Immunocompetence, Int. J. Mol. Sci. 22 (2021) 3847, https://doi.org/10.3390/ijms22083847.

[9] B. Nieuwenhuis, B. Haenzi, M.R. Andrews, J. Verhaagen, J.W. Fawcett, Integrins promote axonal regeneration after injury of the nervous system: Integrins and axonal regeneration, Integrins promote axonal regeneration after injury of the nervous system 93 (3) (2018) 1339–1362.

[10] R. You, Q. Zhang, X. Li, S. Yan, Z. Luo, J. Qu, M. Li, Multichannel Bioactive Silk Nanofiber Conduits Direct and Enhance Axonal Regeneration after Spinal Cord Injury, ACS Biomater. Sci. Eng. 6 (2020) 4677–4686, https://doi.org/10.1021/acsbiomaterials.0c00698.

[11] M. Rahmati, D.K. Mills, A.M. Urbanska, M.R. Saeb, J.R. Venugopal, S. Ramakrishna, M. Mozafari, Progress in Materials Science Electrospinning for tissue engineering applications, Prog. Mater. Sci. 117 (2021) 100721.

[12] Y. Wu, Electrohydrodynamic jet 3D printing in biomedical applications, Acta Biomater. 128 (2021) 21–41, https://doi.org/10.1016/j.actbio.2021.04.036.

[13] M. Ermis, E. Antmen, V. Hasirci, Micro and Nanofabrication methods to control cell-substrate interactions and cell behavior: A review from the tissue engineering perspective, Bioact. Mater. 3 (2018) 355–369, https://doi.org/10.1016/j.bioactmat.2018.05.005.

[14] A. Béduer, C. Vieu, F. Arnauduc, J.C. Sol, I. Loubinoux, L. Vaysse, Engineering of adult human neural stem cells differentiation through surface micropatterning, Biomaterials. 33 (2012) 504–514, https://doi.org/10.1016/j.biomaterials.2011.09.073.

[15] B. Feng, T. Ji, X. Wang, W. Fu, L. Ye, H. Zhang, F. Li, Engineering cartilage tissue based on cartilage-derived extracellular matrix cECM/PCL hybrid nanofibrous scaffold, Mater. Des. 193 (2020), 108773, https://doi.org/10.1016/j.matdes.2020.108773.

[16] R. Deng, Z. Luo, Z. Rao, Z. Lin, S. Chen, J. Zhou, Q. Zhu, X. Liu, Y. Bai, D. Quan, Decellularized Extracellular Matrix Containing Electrospun Fibers for Nerve Regeneration: A Comparison Between Core-Shell Structured and Preblended Composites, Adv. Fiber Mater. 4 (2022) 503–519, https://doi.org/10.1007/s42765-021-00124-5.

[17] M. Nune, M. Bhat, A. Nagarajan, Design of ECM Functionalized Polycaprolactone Aligned Nanofibers for Peripheral Nerve Tissue Engineering, J. Med. Biol. Eng. 42 (2022) 147–156, https://doi.org/10.1007/s40846-022-00699-3.

[18] X. Wen, Y. Wang, Z. Guo, H. Meng, J. Huang, L. Zhang, B. Zhao, Q. Zhao, Y. Zheng, J. Peng, Cauda Equina-Derived Extracellular Matrix for Fabrication of Nanostructured Hybrid Scaffolds Applied to Neural Tissue Engineering, Tissue Eng. Part A 21 (2015) 1095–1105, https://doi.org/10.1089/ten.tea.2014.0173.

[19] G.A.A. Saracino, D. Cigognini, D. Silva, A. Caprini, F. Gelain, Nanomaterials design and tests for neural tissue engineering, Chem. Soc. Rev. 42 (2013) 225–262, https://doi.org/10.1039/C2CS35065C.

[20] Y.J. Hong, J.T. Do, Neural Lineage Differentiation From Pluripotent Stem Cells to Mimic Human Brain Tissues, Front. Bioeng, Biotechnol. 7 (2019) 1–17, https://doi.org/10.3389/fbioe.2019.00400.

[21] A.M. Thomas, M.B. Kubilius, S.J. Holland, S.K. Seidlits, R.M. Boehler, A. J. Anderson, B.J. Cummings, L.D. Shea, Channel density and porosity of degradable bridging scaffolds on axon growth after spinal injury, Biomaterials. 34 (2013) 2213–2220, https://doi.org/10.1016/j.biomaterials.2012.12.002.

[22] K.M. Koss, L.D. Unsworth, Neural tissue engineering: Bioresponsive nanoscaffolds using engineered self-assembling peptides, Acta Biomater. 44 (2016) 2–15, https://doi.org/10.1016/j.actbio.2016.08.026.

[23] T. Liu, J.D. Houle, J. Xu, B.P. Chan, S.Y. Chew, Nanofibrous Collagen Nerve Conduits for Spinal Cord Repair, Tissue Eng. Part A 18 (2012) 1057–1066, https://doi.org/10.1089/ten.tea.2011.0430.

[24] C. Chen, J. Tang, Y. Gu, L. Liu, X. Liu, L. Deng, C. Martins, B. Sarmento, W. Cui, L. Chen, Bioinspired Hydrogel Electrospun Fibers for Spinal Cord Regeneration, Adv. Funct. Mater. 29 (2019) 1806899, https://doi.org/10.1002/adfm.201806899.

[25] A.F. Girão, J. Sousa, A. Domínguez-Bajo, A. González-Mayorga, I. Bdikin, E. Pujades-Otero, N. Casañ-Pastor, M.J. Hortigüela, G. Otero-Irurueta, A. Completo, M.C. Serrano, P.A.A.P. Marques, 3D Reduced Graphene Oxide Scaffolds with a Combinatorial Fibrous-Porous Architecture for Neural Tissue Engineering, ACS Appl. Mater. Interfaces. 12 (2020) 38962–38975, https://doi.org/10.1021/acsami.0c10599.

[26] N. Bakhtiary, M. Pezeshki-Modaress, N. Najmoddin, Wet-electrospinning of nanofibrous magnetic composite 3-D scaffolds for enhanced stem cells neural differentiation, Chem. Eng. Sci. 264 (2022), 118144, https://doi.org/10.1016/j.ces.2022.118144.

[27] Z. Mohammadalizadeh, E. Bahremandi-Toloue, S. Karbasi, Recent advances in modification strategies of pre- and post-electrospinning of nanofiber scaffolds in tissue engineering, React. Funct. Polym. 172 (2022), 105202, https://doi.org/10.1016/j.reactfunctpolym.2022.105202.

[28] M.K. Joshi, H.R. Pant, A.P. Tiwari, H.J. Kim, C.H. Park, C.S. Kim, Multi-layered macroporous three-dimensional nanofibrous scaffold via a novel gas foaming technique, Chem. Eng. J. 275 (2015) 79–88, https://doi.org/10.1016/j.cej.2015.03.121.

[29] X. Jing, H. Li, H.-Y. Mi, Y.-J. Liu, Y.-M. Tan, Fabrication of fluffy shish-kebab structured nanofibers by electrospinning, CO2 escaping foaming and controlled crystallization for biomimetic tissue engineering scaffolds, Chem. Eng. J. 372 (2019) 785–795, https://doi.org/10.1016/j.cej.2019.04.194.

[30] F. Rao, Z. Yuan, M. Li, F. Yu, X. Fang, B. Jiang, Y. Wen, P. Zhang, Expanded 3D nanofibre sponge scaffolds by gas-foaming technique enhance peripheral nerve regeneration, Artif. Cells, Nanomedicine, Biotechnol. 47 (2019) 491–500, https://doi.org/10.1080/21691401.2018.1557669.

[31] A.F. Girão, M.C. Serrano, A. Completo, P.A.A.P. Marques, Is Graphene Shortening the Path toward Spinal Cord Regeneration? ACS Nano. 16 (2022) 13430–13467, https://doi.org/10.1021/acsnano.2c04756.

[32] F. Luo, K. Wu, J. Shi, X. Du, X. Li, L. Yang, M. Lu, Green reduction of graphene oxide by polydopamine to a construct flexible film: superior flame retardancy and high thermal conductivity, J. Mater. Chem. A. 5 (2017) 18542–18550, https://doi.org/10.1039/C7TA04740A.

[33] X.-P. Li, K.-Y. Qu, B. Zhou, F. Zhang, Y.-Y. Wang, O.D. Abodunrin, Z. Zhu, N.-P. Huang, Electrical stimulation of neonatal rat cardiomyocytes using conductive polydopamine-reduced graphene oxide-hybrid hydrogels for constructing cardiac microtissues, Colloids Surfaces B Biointerfaces. 205 (2021), 111844, https://doi.org/10.1016/j.colsurfb.2021.111844.

[34] P. Flouda, S.A. Shah, D.C. Lagoudas, M.J. Green, J.L. Lutkenhaus, Highly Multifunctional Dopamine-Functionalized Reduced Graphene Oxide Supercapacitors, Matter. 1 (2019) 1532–1546, https://doi.org/10.1016/j.matt.2019.09.017.

[35] N. Huang, S. Zhang, L. Yang, M. Liu, H. Li, Y. Zhang, S. Yao, Multifunctional Electrochemical Platforms Based on the Michael Addition/Schiff Base Reaction of Polydopamine Modified Reduced Graphene Oxide: Construction and Application, ACS Appl. Mater. Interfaces. 7 (2015) 17935–17946, https://doi.org/10.1021/acsami.5b04597.

[36] L.Q. Xu, W.J. Yang, K.-G. Neoh, E.-T. Kang, G.D. Fu, Dopamine-Induced Reduction and Functionalization of Graphene Oxide Nanosheets, Macromolecules. 43 (2010) 8336–8339, https://doi.org/10.1021/ma101526k.

[37] W. Li, T. Shang, W. Yang, H. Yang, S. Lin, X. Jia, Q. Cai, X. Yang, Effectively Exerting the Reinforcement of Dopamine Reduced Graphene Oxide on Epoxy-Based Composites via Strengthened Interfacial Bonding, ACS Appl. Mater. Interfaces. 8 (2016) 13037–13050, https://doi.org/10.1021/acsami.6b02496.

[38] C. Silva, F. Simon, P. Friedel, P. Pötschke, C. Zimmerer, Elucidating the Chemistry behind the Reduction of Graphene Oxide Using a Green Approach with Polydopamine, Nanomaterials. 9 (2019) 902, https://doi.org/10.3390/nano9060902.

[39] B. Ribeiro, B. Cruz, B.M. de Sousa, P.D. Correia, N. David, C. Rocha, R. de Almeida, M.R. da Cunha, A.A. Marques Baptista, S.I. Vieira, Cell therapies for spinal cord injury: a review of the clinical trials and cell-type therapeutic potential, Brain 146 (2023) 2672–2693, https://doi.org/10.1093/brain/awad047.

[40] W. Guo, X. Zhang, J. Zhai, J. Xue, The roles and applications of neural stem cells in spinal cord injury repair, Front. Bioeng, Biotechnol. 10 (2022) 1–18, https://doi.org/10.3389/fbioe.2022.966866.

[41] Y. Chen, M. Shafiq, M. Liu, Y. Morsi, X. Mo, Advanced fabrication for electrospun three-dimensional nanofiber aerogels and scaffolds, Bioact. Mater. 5 (2020) 963–979, https://doi.org/10.1016/j.bioactmat.2020.06.023.

[42] M.Y. Abdel Tawwab, B.M. Abdel-Hady, R.A. El-Moneim Rizk, M.W. Shafaa, Effect of electrospinning parameters on the versatile production of polycaprolacton/gelatin nanofibre mats, Adv. Nat. Sci. Nanosci. Nanotechnol. 10 (2019), 025009, https://doi.org/10.1088/2043-6254/ab1fe8.

[43] E. Antaby, K. Klinkhammer, L. Sabantina, Electrospinning of Chitosan for Antibacterial Applications—Current Trends, Appl. Sci. 11 (2021) 11937, https://doi.org/10.3390/app112411937.

[44] I.K. Kwon, T. Matsuda, Co-Electrospun Nanofiber Fabrics of Poly(<scp>l</scp>-lactide- *co* -ε-caprolactone) with Type I Collagen or Heparin, Biomacromolecules. 6 (2005) 2096–2105, https://doi.org/10.1021/bm050086u.

[45] J. Lee, G. Tae, Y.H. Kim, I.S. Park, S.-H. Kim, S.H. Kim, The effect of gelatin incorporation into electrospun poly(l-lactide-co-ε-caprolactone) fibers on mechanical properties and cytocompatibility, Biomaterials. 29 (2008) 1872–1879, https://doi.org/10.1016/j.biomaterials.2007.12.029.

[46] H. Kenar, C.Y. Ozdogan, C. Dumlu, E. Doger, G.T. Kose, V. Hasirci, Microfibrous scaffolds from poly(l-lactide-co-ε-caprolactone) blended with xeno-free collagen/hyaluronic acid for improvement of vascularization in tissue engineering applications, Mater. Sci. Eng. C. 97 (2019) 31–44, https://doi.org/10.1016/j.msec.2018.12.011.

[47] E. Lih, K.W. Park, S.Y. Chun, H. Kim, T.G. Kwon, Y.K. Joung, D.K. Han, Biomimetic Porous PLGA Scaffolds Incorporating Decellularized Extracellular Matrix for Kidney Tissue Regeneration, ACS Appl. Mater. Interfaces. 8 (2016) 21145–21154, https://doi.org/10.1021/acsami.6b03771.

[48] V.Y. Chakrapani, A. Gnanamani, V.R. Giridev, M. Madhusoothanan, G. Sekaran, Electrospinning of type I collagen and PCL nanofibers using acetic acid, J. Appl. Polym. Sci. 125 (2012) 3221–3227, https://doi.org/10.1002/app.36504.

[49] K.-Y. Law, Definitions for Hydrophilicity, Hydrophobicity, and Superhydrophobicity: Getting the Basics Right, J. Phys. Chem. Lett. 5 (2014) 686–688, https://doi.org/10.1021/jz402762h.

[50] T.T. Chau, W.J. Bruckard, P.T.L. Koh, A.V. Nguyen, A review of factors that affect contact angle and implications for flotation practice, Adv. Colloid Interface Sci. 150 (2009) 106–115, https://doi.org/10.1016/j.cis.2009.07.003.

[51] Y.S. Kim, M. Majid, A.J. Melchiorri, A.G. Mikos, Applications of decellularized extracellular matrix in bone and cartilage tissue engineering, Bioeng. Transl. Med. 4 (2019) 83–95, https://doi.org/10.1002/btm2.10110.

[52] T. Li, L. Tian, S. Liao, X. Ding, S.A. Irvine, S. Ramakrishna, Fabrication, mechanical property and in vitro evaluation of poly (L-lactic acid-co-ε-caprolactone) core-shell nanofiber scaffold for tissue engineering, J. Mech. Behav. Biomed. Mater. 98 (2019) 48–57, https://doi.org/10.1016/j.jmbbm.2019.06.003.

[53] Y. Chen, W. Xu, M. Shafiq, J. Tang, J. Hao, X. Xie, Z. Yuan, X. Xiao, Y. Liu, X. Mo, Three-dimensional porous gas-foamed electrospun nanofiber scaffold for cartilage regeneration, J. Colloid Interface Sci. 603 (2021) 94–109, https://doi.org/10.1016/j.jcis.2021.06.067.

[54] K. Zhang, X. Bai, Z. Yuan, X. Cao, X. Jiao, Y. Li, Y. Qin, Y. Wen, X. Zhang, Layered nanofiber sponge with an improved capacity for promoting blood coagulation and wound healing, Biomaterials. 204 (2019) 70–79, https://doi.org/10.1016/j.biomaterials.2019.03.008.

[55] I. Bružauskaitė, D. Bironaitė, E. Bagdonas, E. Bernotienė, Scaffolds and cells for tissue regeneration: different scaffold pore sizes—different cell effects, Cytotechnology. 68 (2016) 355–369, https://doi.org/10.1007/s10616-015-9895-4.

[56] W.Q. Sun, H. Xu, M. Sandor, J. Lombardi, Process-induced extracellular matrix alterations affect the mechanisms of soft tissue repair and regeneration, J. Tissue Eng. 4 (2013), https://doi.org/10.1177/2041731413505305.

[57] D.I. Zeugolis, S.T. Khew, E.S.Y. Yew, A.K. Ekaputra, Y.W. Tong, L.-Y.-L. Yung, D. W. Hutmacher, C. Sheppard, M. Raghunath, Electro-spinning of pure collagen nano-fibres – Just an expensive way to make gelatin? Biomaterials. 29 (2008) 2293–2305, https://doi.org/10.1016/j.biomaterials.2008.02.009.

[58] C.A. Miles, T.V. Burjanadze, A.J. Bailey, The Kinetics of the Thermal Denaturation of Collagen in Unrestrained Rat Tail Tendon Determined by Differential Scanning Calorimetry, J. Mol. Biol. 245 (1995) 437–446, https://doi.org/10.1006/jmbi.1994.0035.

[59] A. Ozcelikkale, B. Han, X. He, Thermal Destabilization of Collagen Matrix Hierarchical Structure by Freeze/Thaw, PLoS One. 11 (1) (2016) e0146660.

[60] P.L. Gordon, C. Huang, R.C. Lord, I.V. Yannas, The Far-Infrared Spectrum of Collagen, Macromolecules. 7 (1974) 954–956, https://doi.org/10.1021/ma60042a052.

[61] B.S. Jha, C.E. Ayres, J.R. Bowman, T.A. Telemeco, S.A. Sell, G.L. Bowlin, D. G. Simpson, Electrospun Collagen: A Tissue Engineering Scaffold with Unique Functional Properties in a Wide Variety of Applications, J. Nanomater. 2011 (2011) 1–15, https://doi.org/10.1155/2011/348268.

[62] C.E. Dorrier, D. Aran, E.A. Haenelt, R.N. Sheehy, K.K. Hoi, L. Pintarić, Y. Chen, C. O. Lizama, K.M. Cautivo, G.A. Weiner, B. Popko, S.P.J. Fancy, T.D. Arnold, R. Daneman, CNS fibroblasts form a fibrotic scar in response to immune cell infiltration, Nat. Neurosci. 24 (2021) 234–244, https://doi.org/10.1038/s41593-020-00770-9.

[63] A. Domínguez-Bajo, A. González-Mayorga, C.R. Guerrero, F.J. Palomares, R. García, E. López-Dolado, M.C. Serrano, Myelinated axons and functional blood vessels populate mechanically compliant rGO foams in chronic cervical hemisected rats, Biomaterials. 192 (2019) 461–474, https://doi.org/10.1016/j.biomaterials.2018.11.024.

[64] A.S. Jack, C. Hurd, J. Martin, K. Fouad, Electrical Stimulation as a Tool to Promote Plasticity of the Injured Spinal Cord, J. Neurotrauma. 37 (2020) 1933–1953, https://doi.org/10.1089/neu.2020.7033.

[65] C. Bertucci, R. Koppes, C. Dumont, A. Koppes, Neural responses to electrical stimulation in 2D and 3D in vitro environments, Brain Res. Bull. 152 (2019) 265–284, https://doi.org/10.1016/j.brainresbull.2019.07.016.

[66] J. Wang, Y. Cheng, L. Chen, T. Zhu, K. Ye, C. Jia, H. Wang, M. Zhu, C. Fan, X. Mo, In vitro and in vivo studies of electroactive reduced graphene oxide-modified nanofiber scaffolds for peripheral nerve regeneration, Acta Biomater. 84 (2019) 98–113, https://doi.org/10.1016/j.actbio.2018.11.032.

[67] R.W. DeBry, M.F. Seldin, Human/Mouse Homology Relationships, Genomics. 33 (1996) 337–351, https://doi.org/10.1006/geno.1996.0209.

[68] P. Assinck, G.J. Duncan, B.J. Hilton, J.R. Plemel, W. Tetzlaff, Cell transplantation therapy for spinal cord injury, Nat. Neurosci. 20 (2017) 637–647, https://doi.org/10.1038/nn.4541.

[69] A. Magaz, X. Li, J.E. Gough, J.J. Blaker, Graphene oxide and electroactive reduced graphene oxide-based composite fibrous scaffolds for engineering excitable nerve tissue, Mater. Sci. Eng. C. 119 (2021), 111632, https://doi.org/10.1016/j.msec.2020.111632.

[70] B.M. Baker, C.S. Chen, Deconstructing the third dimension – how 3D culture microenvironments alter cellular cues, J. Cell Sci. 125 (2012) 3015–3024, https://doi.org/10.1242/jcs.079509.

[71] D. Carradori, J. Eyer, P. Saulnier, V. Préat, A. des Rieux, The therapeutic contribution of nanomedicine to treat neurodegenerative diseases via neural stem cell differentiation, Biomaterials. 123 (2017) 77–91. https://doi.org/10.1016/j.biomaterials.2017.01.032.

[72] E. Dráberová, L. Del Valle, J. Gordon, V. Marková, B. Šmejkalová, L. Bertrand, J.-P. de Chadarévian, D.P. Agamanolis, A. Legido, K. Khalili, P. Dráber, C.D. Katsetos, Class III β-Tubulin Is Constitutively Coexpressed With Glial Fibrillary Acidic Protein and Nestin in Midgestational Human Fetal Astrocytes: Implications for Phenotypic Identity, J. Neuropathol. Exp. Neurol. 67 (2008) 341–354, https://doi.org/10.1097/NEN.0b013e31816a686d.

[73] W. Guo, S. Wang, X. Yu, J. Qiu, J. Li, W. Tang, Z. Li, X. Mou, H. Liu, Z. Wang, Construction of a 3D rGO–collagen hybrid scaffold for enhancement of the neural differentiation of mesenchymal stem cells, Nanoscale. 8 (2016) 1897–1904, https://doi.org/10.1039/C5NR06602F.

[74] M. Catanesi, G. Panella, E. Benedetti, G. Fioravanti, F. Perrozzi, L. Ottaviano, L. D. Leandro, M. Ardini, F. Giansanti, M. d'Angelo, V. Castelli, F. Angelucci, R. Ippoliti, A. Cimini, YAP/TAZ mechano-transduction as the underlying mechanism of neuronal differentiation induced by reduced graphene oxide, Nanomedicine. 13 (24) (2018) 3091–3106.

[75] K. Yang, J.S. Lee, J. Kim, Y. Bin Lee, H. Shin, S.H. Um, J.B. Kim, K.I. Park, H. Lee, S.-W. Cho, Polydopamine-mediated surface modification of scaffold materials for human neural stem cell engineering, Biomaterials. 33 (2012) 6952–6964, https://doi.org/10.1016/j.biomaterials.2012.06.067.

[76] M. Clagett-Dame, E.M. McNeill, P.D. Muley, Role of all-trans retinoic acid in neurite outgrowth and axonal elongation, J. Neurobiol. 66 (2006) 739–756, https://doi.org/10.1002/neu.20241.

[77] J.F. Da Rocha, O.A.B. Da Cruz, E. Silva, S.I. Vieira, Analysis of the amyloid precursor protein role in neuritogenesis reveals a biphasic SH-SY5Y neuronal cell differentiation model, J. Neurochem. 134 (2015) 288–301, https://doi.org/10.1111/jnc.13133.

[78] S. Ahmed, B. Reynolds, S. Weiss, BDNF enhances the differentiation but not the survival of CNS stem cell- derived neuronal precursors, J. Neurosci. 15 (1995) 5765–5778, https://doi.org/10.1523/JNEUROSCI.15-08-05765.1995.

[79] L. Dehmelt, S. Halpain, Protein family review The MAP2 / Tau family of microtubule-associated proteins, (2004) 1–10. https://doi.org/https://doi.org/10.1186/gb-2004-6-1-204.

[80] D. Neves, B.J. Goodfellow, S.I. Vieira, R.M. Silva, The role of NAD metabolism in neuronal differentiation, Neurochem. Int. 159 (2022), 105402, https://doi.org/10.1016/j.neuint.2022.105402.

[81] B. Shafit-Zagardo, N. Kalcheva, Making sense of the multiple MAP-2 transcripts and their role in the neuron, Mol. Neurobiol. 16 (1998) 149–162, https://doi.org/10.1007/BF02740642.

[82] T. Shirao, The Roles of Microfilament-Associated Proteins, Drebrins, in Brain Morphogenesis: A Review, J. Biochem. 117 (1995) 231–236, https://doi.org/10.1093/jb/117.2.231.

[83] W.J. Chung, S. Kindler, C. Seidenbecher, C.C. Garner, MAP2a, an Alternatively Spliced Variant of Microtubule-Associated Protein 2, J. Neurochem. 66 (2002) 1273–1281, https://doi.org/10.1046/j.1471-4159.1996.66031273.x.